Rapid attribution analysis of the extraordinary heatwave on the Pacific Coast of the US and Canada June 2021

Sjoukje Y. Philip[1,*], Sarah F. Kew[1,*], Geert Jan van Oldenborgh[1,2,†], Faron S. Anslow[3], Sonia I. Seneviratne[4], Robert Vautard[5], Dim Coumou[1,6], Kristie L. Ebi[7], Julie Arrighi[8,9,10], Roop Singh[8], Maarten van Aalst[8,9,11], Carolina Pereira Marghidan[9], Michael Wehner[12], Wenchang Yang[13], Sihan Li[14], Dominik L. Schumacher[4], Mathias Hauser[4], Rémy Bonnet[5], Linh N. Luu[1], Flavio Lehner[15,16], Nathan Gillett[17], Jordis S. Tradowsky[18,19], Gabriel A. Vecchi[13,20], Chris Rodell[21], Roland B. Stull[21], Rosie Howard[21], and Friederike E. L. Otto[14]

[1]Royal Netherlands Meteorological Institute (KNMI), De Bilt, The Netherlands
[*]These authors contributed equally to this work.
[2]Atmospheric, Oceanic and Planetary Physics, University of Oxford, UK
[†]deceased, 12 October 2021
[3]Pacific Climate Impacts Consortium, University of Victoria, Victoria, V8R4J1, Canada
[4]Institute for Atmospheric and Climate Science, Department of Environmental Systems Science, ETH Zurich, Zurich, Switzerland
[5]Institut Pierre-Simon Laplace, CNRS, Sorbonne Université, Paris, France
[6]Institute for Environmental Studies (IVM), VU Amsterdam, The Netherlands
[7]Center for Health and the Global Environment, University of Washington, Seattle WA, USA
[8]Red Cross Red Crescent Climate Centre, The Hague, the Netherlands
[9]Faculty of Geo-Information Science and Earth Observation (ITC), University of Twente, Enschede, the Netherlands
[10]Global Disaster Preparedness Center, American Red Cross, Washington DC, USA
[11]International Research Institute for Climate and Society, Columbia University, New York, USA
[12]Lawrence Berkeley National Laboratory, Berkeley, California USA
[13]Department of Geosciences, Princeton University, Princeton, 08544, USA
[14]School of Geography and the Environment, University of Oxford, UK
[15]Department of Earth and Atmospheric Sciences, Cornell University, USA
[16]Climate and Global Dynamics Laboratory, National Center for Atmospheric Research, USA
[17]Canadian Centre for Climate Modelling and Analysis, Environment and Climate Change Canada, Victoria, BC, Canada
[18]Deutscher Wetterdienst, Regionales Klimabüro Potsdam, Potsdam, Germany
[19]Bodeker Scientific, Alexandra, New Zealand
[20]The High Meadows Environmental Institute, Princeton University, Princeton, 08544, USA
[21]Department of Earth, Ocean, and Atmospheric Sciences, The University of British Columbia, Vancouver, Canada

Correspondence: Sjoukje Philip (sjoukje.philip@knmi.nl); Sarah Kew (sarah.kew@knmi.nl)

Abstract. Towards the end of June 2021, temperature records were broken by several degrees Celsius in several cities in the Pacific northwest areas of the U.S. and Canada, leading to spikes in sudden deaths, and sharp increases in emergency calls and hospital visits for heat-related illnesses. Here we present a multi-model, multi-method attribution analysis to investigate to what extent human-induced climate change has influenced the probability and intensity of extreme heatwaves in this region.

5 Based on observations, modeling and a classical statistical approach the occurrence of a heatwave defined as the maximum daily temperatures (TXx) observed in the area 45 °N–52 °N, 119 °W–123 °W, was found to be virtually impossible without

human-caused climate change. The observed temperatures were so extreme that they lie far outside the range of historical temperature observations. This makes it hard to quantify with confidence how rare the event was. Using a statistical analysis that assumes that the heatwave is part of the same distribution as previous heatwaves, i.e. it can be included in the statistical fit and it was not intensified by new nonlinearities, a first order estimation of the event frequency is of the order of once in 1000 years under current climate conditions. Using this assumption and in combining the results from the analysis of climate models and weather observations, we find that such a heat event would be at least 150 times less common without human-induced climate change. Also, this heatwave was about 2°C hotter than a 1 in 1000-year heatwave would have been at the beginning of the industrial revolution, when global mean temperatures were 1.2°C cooler than today. Looking into the future, in a world with 2°C of global warming (0.8°C warmer than today), a 1000-year event would be another degree hotter. Our results provide a strong warning: our rapidly warming climate is bringing us into uncharted territory with significant consequences for health, well-being, and livelihoods. Adaptation and mitigation are urgently needed to prepare societies for a very different future.

1   Introduction

During the last days of June 2021, Pacific northwest areas of the U.S. and Canada experienced temperatures never previously observed, with temperature records broken in multiple cities by several degrees Celsius. Temperatures far above 40 °C (104 °F) occurred on Sunday 27 to Tuesday 29 June (Figs 1a,b for Monday) in the Pacific northwest areas of the U.S. and western Provinces of Canada, with the maximum warmth moving from the western to the eastern part of the domain from Monday to Tuesday. The anomalies relative to the maximum temperature climatology for the time of year reached 16°C to 20 °C (Figs 1c,d). It is noteworthy that these record temperatures occurred one whole month before the climatologically warmest part of the year (end of July, early August), making them particularly exceptional. Even compared to the maximum temperatures in other years independent of the considered month, the recent event exceeds those temperatures by about 5 °C (Figure 2). Records were shattered in a very large area, including setting a new all-time Canadian temperature record in the village of Lytton, at which a temperature of 49.6 °C was measured on June 29 and where wildfires spread on the following day.

Given that the observed temperatures were so far outside historical experiences and occurred in a region with only about 50% household air conditioning penetration, large impacts on health were expected. In British Columbia, Canada, there were an estimated 740 heat-related excess deaths putting the event among the deadliest weather related events in Canada (Henderson et al., 2021). There were nearly 450 extra deaths in Washington and nearly 160 in Oregon.[1]

Below we investigate the role of human-induced climate change in contributing to the likelihood and intensity of this extreme heatwave, following an established approach to multi-model multi-method extreme event attribution (Philip et al., 2020; van Oldenborgh et al., 2021). We focus the analysis on the maximum temperatures in the region where most people were affected by the heat (45 °N–52 °N, 119 °W–123 °W) including the cities of Seattle, Portland, and Vancouver. While the extreme heat was an important driver of the observed impacts, it is important to note that these impacts strongly depend on exposure, vulnerability, and other climatological variables beyond temperature. In addition to the attribution of the extreme temperatures

---

[1]https://www.nytimes.com/interactive/2021/08/11/climate/deaths-pacific-northwest-heat-wave.html

Maximum temperature
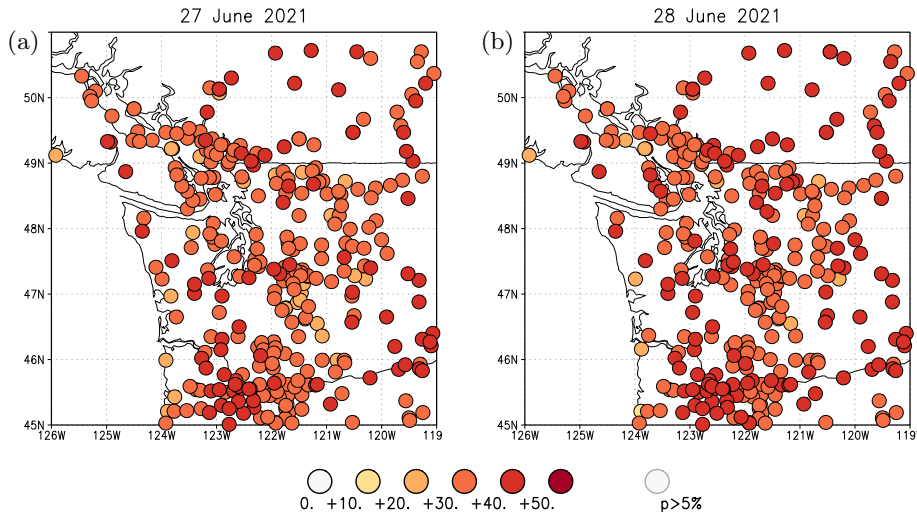
Maximum temperature anomaly
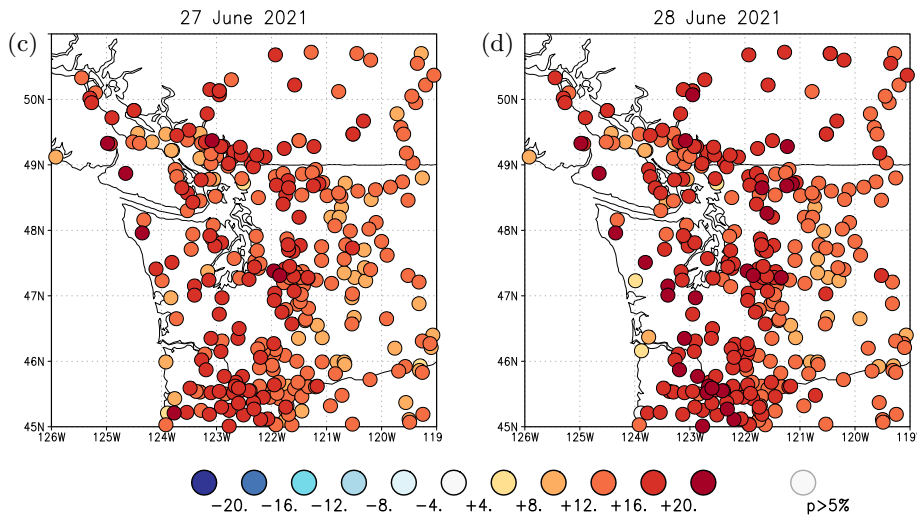
Figure 1. a) observed temperatures on 27 June 2021, b) 28 June 2021, c,d) same for anomalies relative to the whole station records. Source: GHCN-D

we qualitatively assess whether meteorological drivers and antecedent conditions played an important role in the observed

40   extreme temperatures in Section 6.
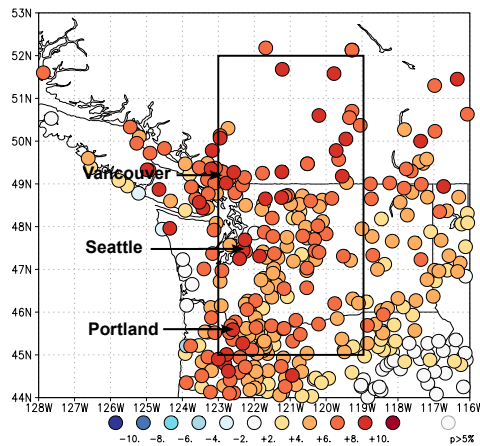
Figure 2. Anomalies of 2021 highest daily maximum temperature (TXx) relative to the whole time series of each station. The black box indicates the study region. Source: GHCN-D

1.1 Event definition

For the attribution analysis, a definition of the event is required. As there are several options to define an event, this step requires some expert judgment. Within this study, we will analyse the daily maximum temperatures, which characterised the event and were the headline figure in the large number of media reports describing the heatwave and it?s associated impacts. We therefore
45 define the event based on the annual maximum of daily maximum temperature, TXx. Here, we first average over the region and then take the annual maximum. Other options for variables that could be selected for analysis include e.g. 3-day averaged temperatures, as there is some evidence that longer time scales better describe the health impacts (e.g., D'Ippoliti et al., 2010) or high minimum temperatures which also have strong impacts on human health. However, TXx is a standard heat impact index and thus the results can easily be compared to other studies. We intentionally focus on one event definition to keep this analysis
50 succinct and its results easy to communicate, choosing TXx, which not only characterises the extreme character of the event but is also readily available in climate models allowing us to use a large range of different models. Recognising that the WMO standard definition of a heatwave is a multi-day measure associated with persistent heat, we additionally considered the annual maxima of 5-day and 10-day averages of daily maximum temperatures, TX5x and TX10x, for observations. Trends in these time series, as seen by the intensity change, turn out to be very similar to the results for TXx presented in Sect. 3. As the spatial
55 scale of the event we consider the area 45°N–52°N, 119°W–123°W. This covers the more populated region around Portland, Seattle and Vancouver that were impacted heavily by the heat (with a total population of over 9.4 million in their combined metropolitan areas), but excludes the rainforest to the west and arid areas to the east. Note that this spatial event definition is based on the expected and reported human impacts rather than on the meteorological extremity. Besides the analysis for this region we also analysed long and homogeneous observational records of three stations in Portland, Seattle and Vancouver.
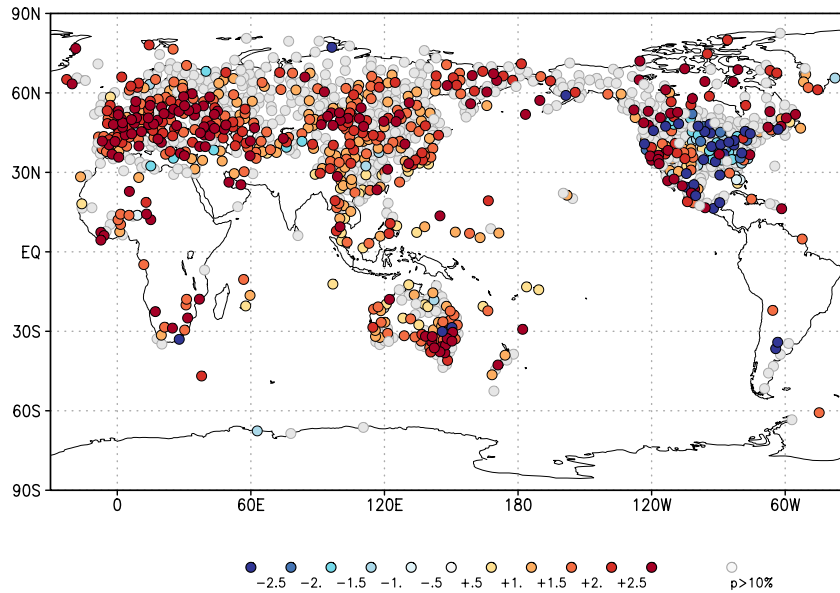
Figure 3. Trends in the highest daily maximum temperature of the year in the GHCN-D station data. Stations are selected to have at least 50 years of data and to be at least 2°apart. The local trends are defined by their regression on the global mean temperature, and shown in units of multiples of the global mean temperature rise. Source: GHCN-D

1.2 Previous trends in heatwaves

Figure 3 shows the observed trends in TXx in the GHCN-D dataset over 1900–2019. The stations were selected on the basis of a long time series, at least 50 years of data, and being at least 2°apart. The trend is defined as the regression on the global mean temperature, so the numbers represent how much slower or faster the temperature has changed compared to the global mean the. Individual stations with different trends than nearby stations usually have inhomogeneities in the observational method or local environment. The negative trends in eastern North America and parts of California are well-understood to be the result of land use changes, irrigation and changes in agricultural practice (Donat et al., 2016, 2017; Thiery et al., 2017; Cowan et al., 2020). The large trends in heatwaves in Europe are not yet fully understood or adequately represented in climate models (Vautard et al., 2020). The Pacific Northwest showed trends twice as large as the global temperature trend up to 2019.

2 Data and methods

2.1 Observational data

The dataset used to represent the heatwave is the ERA5 reanalysis (Hersbach et al., 2019) from ECMWF at 0.25°resolution. A very rapid analysis performed directly after the heatwave and published on https://www.worldweatherattribution.org/

western-north-american-extreme-heat-virtually-impossible-without-human-caused-climate-change/ used ERA5 extended by the ECMWF operational analysis and the ECMWF forecast. The difference in the heatwave amplitude between the rapid analysis and the updated analysis presented here are minor and do not affect the estimated return period used in this study. Therefore, the analysis results do not require to be updated following the availability of the ERA5 data for the event?s timeframe.

Temperature observations were used to assess probability ratios and return periods associated with the event for three major cities in the study area, i.e. Portland, Seattle, and Vancouver. Observing sites were chosen based on (i) the availability of long homogenized historical records, (ii) their ability to represent the severity of the event by avoiding sites within the proximity to large water bodies, and (iii) their representativeness for populous areas of each city to better illuminate impact on inhabitants.

For Portland, the Portland International Airport National Weather Service station was used, which has continuous observations over 1938–2021. The airport is located close to the city centre, adjacent to the Columbia River. The river's influence is thought to be small. For Seattle, Seattle-Tacoma International Airport was chosen, which has almost continuous observations between 1948–2021, among the longest records in the Seattle area. This location is further inland and thus avoids the influence of Lake Washington that affects downtown Seattle. Two long records exist adjacent to downtown Vancouver, but they are both very exposed to the Georgia Strait that influenced observations due to local onshore flow during the peak of the event. Thus the time series from a site further inland at New Westminster was selected, which starts in 1875 but contains data gaps in 1882–1893, 1928, 1980–1993.

The data for Portland International Airport and Seattle-Tacoma International Airport were gathered from the Global Historical Climatology Network Daily (GHCND; Menne et al., 2012) while data for New Westminster were gathered from the Adjusted Homogenized Canadian Climate Dataset (AHCCD) for daily temperature (Vincent et al., 2020). This station's record is a composite of data from three locations in two nearby cities as location changes took place in 1966 and 1980. From 1874 to 1966, the station operated at an elevation of 118 m above sea level near the centre of New Westminster. In 1966, the station was moved about 2 km east and to an elevation of 18 m. The portion of the homogenized record from 1980 onward is from Pitt Meadows, BC, located about 14 km east of the previous location at an elevation of 5 m. Using a composite station is non-ideal given the potential influence of local micro-climatic effects and particularly the increasing distance from theThe Strait of Georgia which exhibits a cooling effect to sites in its vicinity. Use of data from this composite site may increase the uncertainty of our analysis, but given the magnitude of the signal and the consistency of results among the datasets presented here (and analysis of other temperature datasets from BC, not shown here), we accept these issues. The AHCCD dataset is updated annually and ends in 2020. Data for 2021 were appended from unhomogenized recent records from Environment and Climate Change Canada. Overlapping data for 2020 were compared between the two sources and found to be identical except for several duplicate/missing observations. Such duplicate or missing data would not cause error in the present analysis because the records are complete for June 2021.

As a measure of anthropogenic climate change we use the global mean surface temperature (GMST), where GMST is taken from the National Aeronautics and Space Administration (NASA) Goddard Institute for Space Science (GISS) surface temperature analysis (Hansen et al., 2010; Lenssen et al., 2019, GISTEMP,). We apply a 4-yr running mean low-pass filter to suppress the influence of ENSO and winter variability at high northern latitudes as these are unforced variations.

2.2 Model and experiment descriptions

In this study a variety of climate model simulations are analysed and will be described in the following.

Model simulations from the 6th Coupled Model Intercomparison Project (CMIP6; Eyring et al., 2016) are assessed after combining the historical simulations (1850 to 2015) with the Shared Socioeconomic Pathway (SSP) projections (O'Neill et al., 2016) for the years 2016 to 2100. Here, we only use data from SSP5-8.5, noting that SSPs are very similar over the period 2015–2021. Models are excluded if they do not provide the relevant variables, do not run from 1850 to 2100, and if they either include duplicate time steps or miss time steps. All available ensemble members are used. A total of 18 models (88 ensemble members), which fulfill these criteria and passed the validation tests (Section 4), are used.

In addition an ensemble of extended historical simulations from the IPSL-CM6A-LR model is used (see Boucher et al., 2020, for a description of the model), which follows the CMIP6 protocol (Eyring et al., 2016). It is composed of 32 members, and the simulations cover over the historical period (1850-2014). It is extended until 2029 using all forcings from the SSP2-4.5 scenario, except for the ozone concentration which has been kept constant at its 2014 climatology, as it was not available at the time of performing the extensions. This ensemble is used to explore the influence of internal variability.

The GFDL-CM2.5/FLOR (Vecchi et al., 2014) is a fully coupled climate model developed at the Geophysical Fluid Dynamics Laboratory (GFDL). While the ocean and ice components have a horizontal resolution of only $1°$, the resolution of atmosphere and land is about 50 km and might therefore provide a better simulation that coarser model simulations of certain extreme weather events (Baldwin et al., 2019). The data used in this study cover the period from 1860 to 2100, and combine historical and RCP4.5 experiments driven by transient radiative forcings from CMIP5 (Taylor et al., 2011).

We also examine five ensemble members of the AMIP experiment (1871-2019) from the GFDL-AM2.5C360 (Yang et al., 2021; Chan et al., 2021), which consists of the atmosphere and land components of the FLOR model but with finer horizontal resolution of 25 km for a potentially better representation of extreme events.

Further, we use simulations of the Climate of the 20th Century Plus Project (C20C+) project which was designed specifically for event attribution studies (Stone et al., 2019). C20C+ simulations are based on models of the atmosphere and land with prescribed sea surface temperatures and sea ice concentrations, similar to the design of AMIP experiments. To quantify the impact, if any, on extreme events, participating models were run following the AMIP protocol. The distribution of TXx in the study area was examined for three C20C+ models, i.e. CAM5.1, MIROC5 and HadGEM3-A-N216 and compared to that of the ERA5 reanalysis. Only the Community Atmospheric Model (CAM5.1, Neale et al. (2010)), run at $\sim1°$resolution, satisfied the requirements of this study in the statistical description of heat extremes. . The actual world ensemble consists of 99 simulations of mixed duration all ending in 2018, resulting in a sample size of 4090 years. A counterfactual world ensemble of similar size consists of 89 simulations resulting in a sample size of 3823 years.

2.3 Statistical methods

A full description of the statistical methods is given in (Philip et al., 2020; van Oldenborgh et al., 2021). Here we give a summary.

As discussed in Section 1.1, we analyse the annual maximum of daily maximum temperatures (TXx) averaged over 45°N-52°N, 119°W-123°W. Initially, we analyse reanalysis data and station data from sites with long data records. Next, we analyse climate model output of TXx. We follow the steps outlined in the World Weather Attribution (WWA) protocol for event attribution which include: (i) trend calculation from observations; (ii) model validation; (iii) multi-method multi-model attribution and (iv) synthesis of the attribution statement.

For the event under investigation we calculate the return periods, probability ratio (PR) and change in intensity as a function of GMST, where PR is defined as $\mathrm{PR} = p_1/p_0$, with p_1 the probability of an event as strong as or stronger than the extreme event in the current climate and p_0 the probability of such an event in a counterfactual climate without anthropogenic emissions. The two climates we compared are defined as the GMST of the event year 2021 and a GMST value representative of the climate of the late nineteenth century, -1.2 °C relative to 2021 (1850-1900, based on the Global Warming Index https://www.globalwarmingindex.org). To statistically model the selected event, we use a GEV distribution that shifts with GMST, i.e., the location parameter has a term proportional to GMST and the scale and shape parameters are assumed constant. The PRs are calculated from observations and from differentmodels and results are synthesized into a consistent attribution statement. For models (except for IPSL-CM6A-LR and CAM5.1), we additionally analyse the PR between the current climate and a future climate at +2°C above the 1850-1900 reference, which is equivalent to +0.8°C above the current climate of 2021. For this analysis of future change we use model data up to about 2050 or when the model GMST reaches +0.8 °C compared to now.

The CMIP6 data are analysed using the same statistical models as the main method. However, for practical reasons, the parameter uncertainty is estimated in a Bayesian setting using a Markov Chain Monte Carlo (MCMC) sampler instead of a bootstrapping approach (see Ciavarella et al., 2021, for details).

3   Observational analysis: return time and trend

Time series of various aspects of the main index are shown in Figure 4: a) the daily maximum temperature (Tmax) evolution from ERA5 (from 1 May to 31 Aug); and b) annual maximum of the time series. The value for 2021, 39.7 °C, is 5.7 °C above the previous record of 34.0 °C. This extremely large increase leads to difficulties in the statistical analysis described below. There are two possible sources of this extreme jump in peak temperatures. The first is that an event with very low probability occurred — the statistical equivalent of "really bad luck". An event with very low probability could have also occurred in pre-industrial climate but its amplitude would have been aggravated by climate change in the current climate which already includes about 1.2°C of global warming. The second option is that strong nonlinear interactions and feedbacks took place in this event with yet unseen temperatures, relative to previous heatwaves, amplifying the intensity of the extreme, a sign that climate change could exacerbate extreme heatwaves beyond expected temperatures. In this case, the event would not belong to the "same population" as the other ones and we would not expect the method applied here to be successful. This second possibility requires further investigation. While we keep this possibility in mind, we assume the first option within this study.
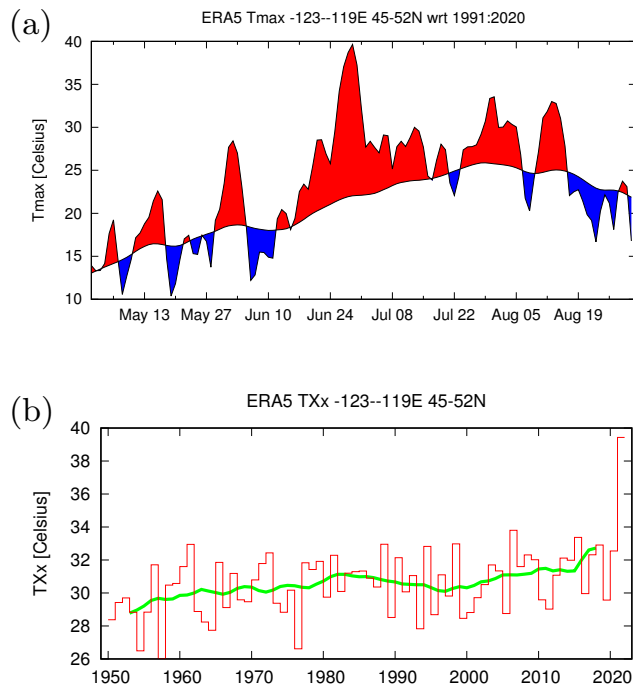
Figure 4. a) Time series for May-Aug 2021 of the maximum daily temperature averaged over the study area based on ERA5, with positive and negative departures from the 1991–2020 climatological mean of daily maximum temperature shaded red and blue, respectively. b) Annual maximum of the index series with a 10-yr running mean (green line). Source: ERA5.

In Figure 5a we show the seasonal cycle of the daily maximum temperature averaged over the index region and in Figure 5b the spatial pattern of TXx averaged over several years individually at each grid point. These two metrics are also used in the model validation procedure, see Section 4.

3.1 Analysis of station and gridded data

Figure 6 shows the standard extreme value evaluation applied for attribution studies within WWA, which in general excludes data of the analysed extreme event from the statistical fit when the study area has been chosen based on the location of the extreme event, to avoid selection bias. Figure 6a shows the observed TXx as a function of smoothed GMST and shows that the value observed in 2021 is far outside the range of any values observed to date. The distribution of TXx including data up to 2020 is described very well by a GEV distribution that has linearly warmed at a rate about twice as fast as the GMST, see Figure 6b. The warming rate is consistent with the expectation as summer temperatures over continents increase faster than the global mean. The GEV fit has a negative shape parameter ξ, which implies a finite tail, and hence an upper bound, here at 35.5$\pm$1.3 °C (2σ uncertainty). However, the value observed in 2021, 39.7 °C, is far above this upper bound. Therefore, this GEV fit with constant shape and scale parameters that excludes all information about 2021 does not provide a valid description of heatwaves in the area.
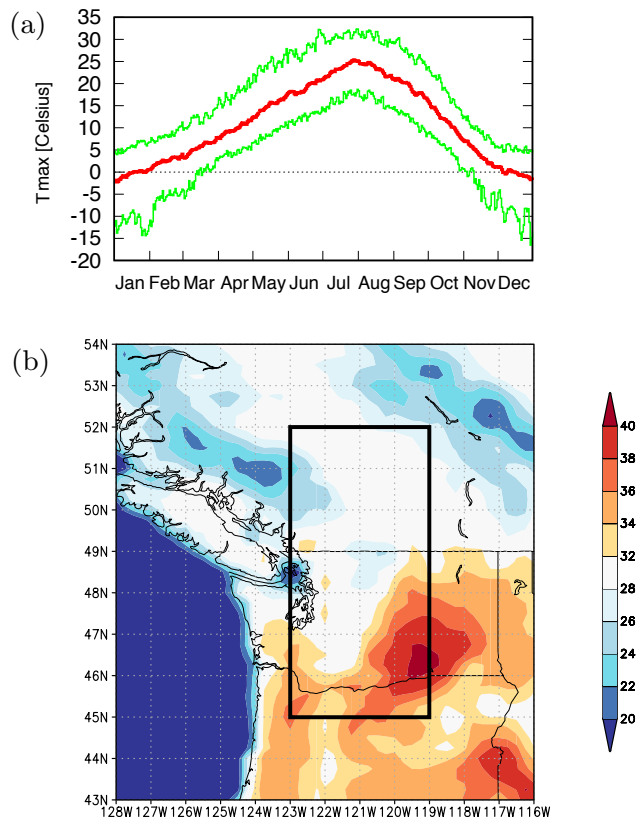
Figure 5. a) Seasonal cycle of Tmax averaged over the land points of 45 °N–52 °N, 119 °N–123 °N, showing the 1950–2021 mean (red) and 2.5% and 97.5% percentiles of the distribution (green). b) Spatial pattern of the 1950–2021 mean of the annual maximum of Tmax (multi-year mean TXx) at each grid point. Source: ERA5.

An alternative to the standard approach for which no information of the event under study is used (to avoid a selection bias), is to use the information that it actually happened, yet without including the value observed in 2021 in the fit. Specifically, we again assume that the data up to 2020 can be described by a GEV distribution with constant scale and shape parameters, but we reject all GEV models in which the upper bound is below the value observed in 2021. In other words, we enforce that the fit parameters are within a subset of parameters that are compatible with the 2021 event. The result is shown in Figure 7. While the distribution now includes the 2021 event, the fit to the data up to and including the year 2020 is noticeably worse than when not taking 2021 into account. The return time for the 2021 event under these assumptions still has a lower bound of 10,000 years in the current climate. The fit differs from the previous one mainly in the shape parameter, which is now much less negative (about -0.2 instead of -0.4). This shifts the upper bound to higher values. The fit also gives a somewhat higher trend parameter.

The third possibility is to fit the GEV distribution over all available data, including observations from 2021. This approach implicitly assumes that the 2021 event is drawn from the same population. We typically do not make this assumption in cases
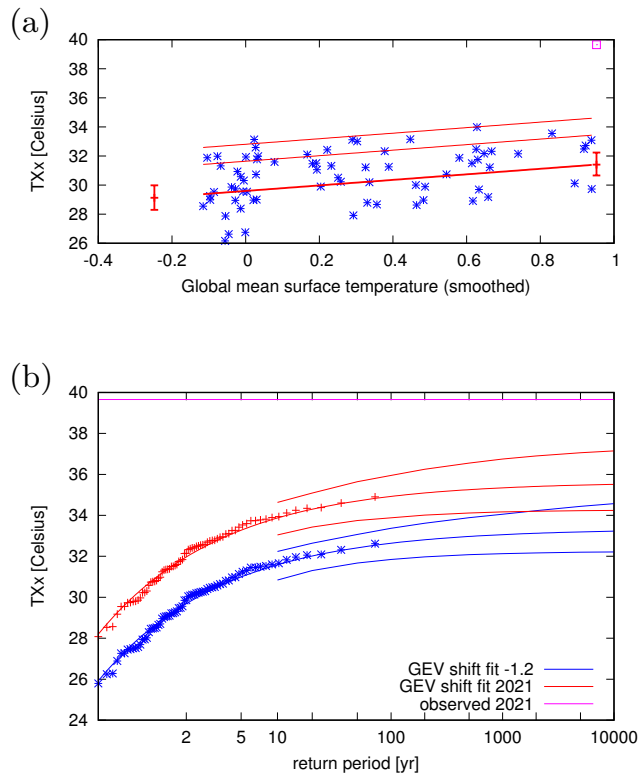
Figure 6. GEV fit with constant scale and shape parameters, and location parameter shifting proportional to GMST of the index series. No information from 2021 is included in the fit. (a): the observed TXx as a function of the smoothed GMST. The thick red line denotes the location parameter, the thin red lines the 6-yr and 40-yr return times. The June 2021 observation is highlighted with the magenta square and is not included in this fit. (b): Return time plots for the climate of 2021 (red) and a climate with GMST 1.2 °C cooler (blue). The red and blue lines indicate the best fit and the 95% confidence intervals, the magenta line shows the observed value. The past observations are shown twice: once shifted up to the current climate and once shifted down to the climate of the late nineteenth century. Source: ERA5, fit: KNMI Climate Explorer.

where we intentionally selected a specific region in order to maximise the extremity (i.e. return period) of the event to avoid
200   a selection bias. In intentionally choosing the region with the largest (rarest) return period for the 2021 event, the extreme value is drawn from a different distribution and cannot be included. However, this is only partly the case here as we did choose the general region because the heat was exceptional there. We based the choice of a subregion for the analysis on population density and type of terrain, parameters that are independent of the heatwave. The benefit of this approach is that it uses all available information. With this approach we still assume this was an event happening by chance.

205   Given the extremity of the event and the relatively low number of data, a robust GEV fit is hard to obtain, and the appropriateness of the method is difficult to assess. However, the application of this classical method in this case is interesting provided we keep in mind the assumptions we make. While we acknowledge that none of the three possibilities to fit a GEV distribution

(a)

(b)
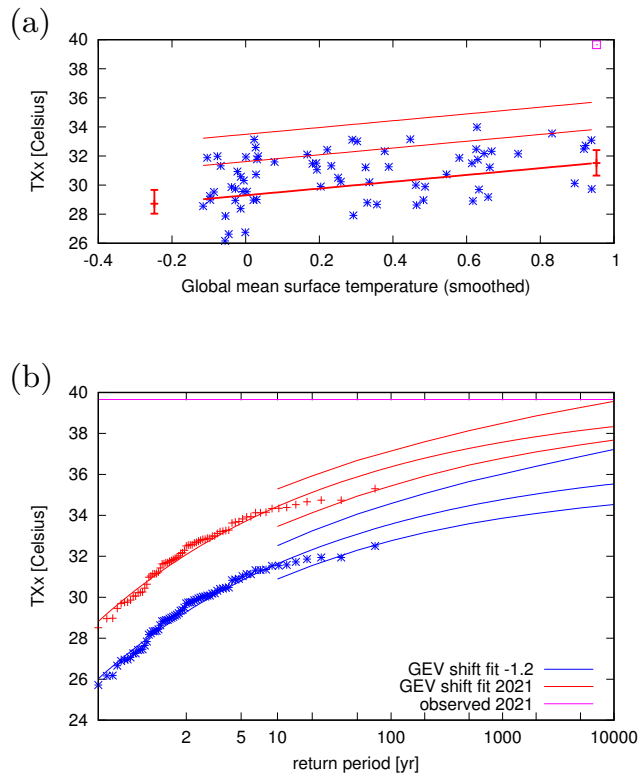
Figure 7. As Figure 6 but demanding the 2021 event is possible in the fitted GEV function, i.e., the upper bound is higher than the value observed in 2021.

is fully satisfying, we decided on using this third approach to estimate the return period leading to an estimate of 1,000 years (95% CI >100 yr). Follow-up research will be necessary to investigate the potential reasons for this outstanding event and the

210 consequences on assumptions for these fits (see also the discussion in Sections 6 and 8). Also, further research is needed into the limitations of standard GEV analysis on annual maxima with short records and seemingly non-stationary behavior. Climate model large ensembles offer a future test bed to investigate the robustness of the method in light of current limitations.

This fit gives a 95% CI of 1.4 K to 1.9 K for the scale parameter σ and -0.5 to 0.0 for the shape parameter ξ. These values are used for the model validation in Section 4.

215 The detection results, i.e., the comparison of the fit for 2021 and for a pre-industrial climate, show an increase in intensity of TXx of $\Delta T = 3.1\,°C$ (95% CI: 1.2 to 4.8 $°C$) and a probability ratio PR of 390 (3.2 to ∞).

3.2 Analysis of temperature in Portland, Seattle and Vancouver

For Portland we chose the International Airport station, which is located on the northern edge of the city and has been collecting data since April 1938; the data are in the GHCN-D v2 database. Figure 9 (top panel) shows the annual maxima of the Portland

(a)

(b)
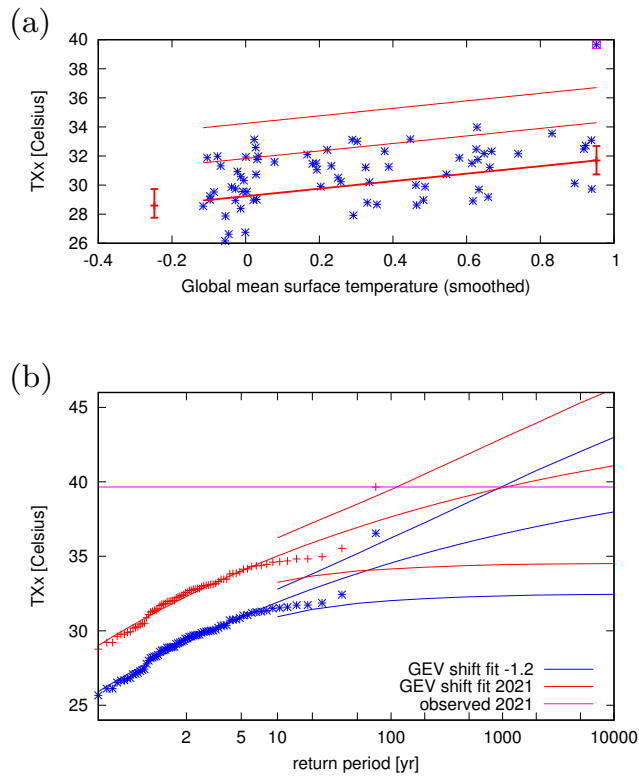
Figure 8. As for Figure 6 but including data from the 2021 heatwave into the fit.

station time series, assuming there will be no higher value during the rest of the year. The record before this year was 41.7 °C in 1965 and 1981, and TXx reached 46.7 °C this year, so the previous record was broken by 5.0 °C.

We fit a GEV distribution to this data, including 2021 (Figure 9, lower panels). It gives a return time of 700 yr for the 2021 event with a lower bound of 70 yr. For the PR we can only give a lower bound of 6, since the best estimate is infinite. This corresponds to an increase in temperature of 3.4 °C with a large uncertainty of 0.3 to 5.3 °C. The large uncertainties are due to the somewhat shorter time series and large variability at this station.

In Seattle, the only station with a sufficiently long time series that includes 2021 is Seattle-Tacoma International Airport. It is located ∼15 km south of the city but has similar terrain, without the proximity to water of the city itself. The previous record was 39.4 °C in 2009, and this year it reached 42.2 °C. This is still a large increase of 2.8 °C over the previous record. The event was also not quite as improbable, with a return time of 300 yr (lower bound 40 yr) in the current climate (Figure 10). The PR is again infinite with a lower bound of 7, and the increase in temperature from a late nineteenth century climate is 3.8 °C (0.7 °C to 5.7 °C).

In the Vancouver area the most representative station with the least missing data is New Westminster. It has data from 1875 to 2021 with a few gaps. The previous record was 37.6 °C in 2009, and in 2021 a temperature of 41.4 °C was observed, 4.0 °C
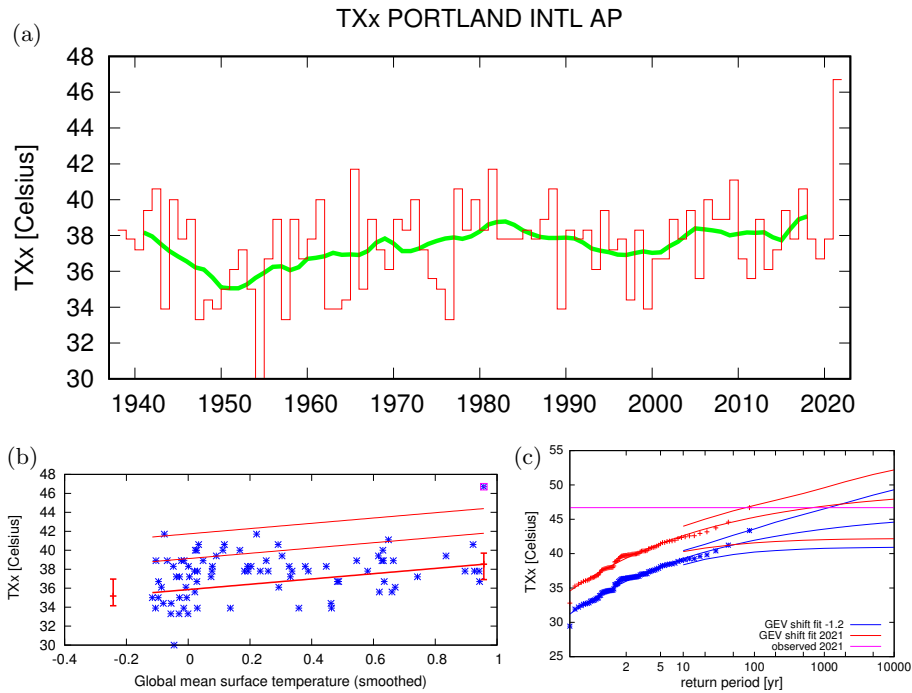
Figure 9. (a) time series of observed highest daily maximum temperature of the year at Portland International Airport. (b,c): as Figure 8 but for the station data at Portland International Airport. Source: data GHCN-D, fit: KNMI Climate Explorer.

warmer. A GEV fit including 2021 gives a return time of 1000 yr with a lower bound of 70 yr (Figure 11). The PR is infinite with a lower bound of 170, and the temperature increased by 3.4 °C (1.9 °C to 5.5 °C).

4 Model evaluation and analysis

In this section we show the results of the model validation. The validation criteria assess the similarity between the modelled and observed seasonal cycle, the spatial pattern of the climatology, and the scale and shape parameters of the GEV distribution. The assessment results in a label "good", "reasonable" or "bad", according to the criteria defined in Ciavarella et al. (2021). In this study, we use models that are labelled "good" or "reasonable". However, if five or more models are classified as "good" within a particular framing such as the CMIP6 models, then we do not include all of the "reasonable" models but only those that pass the specific test on fit parameters as "good". Table 1 shows the model validation results. The full table including the models that did not pass the validation tests is given in Table 3. 21 models and a combined 224 ensemble members passed the validation test.

Next, we show probability ratios and change in intensity ΔT for models that pass the validation tests and also includes the values calculated from the fits to observations (Table 2). Results are given both for changes in current climate (1.2°C) compared

Table 1. Validation results for models that pass the validation tests on seasonal cycle, spatial pattern and fitted GEV scale parameter and shape parameter (sigma). Observations in blue, models in black.

Model / Observations (number of members)	Seasonal cycle	Spatial pattern	Sigma	Shape parameter	Conclusion
ERA5			1.70 (1.40 ... 1.90)	-0.200 (-0.500 ... 0.00)	
GFDL-CM2.5/FLOR historical-rcp45 (5)	good	good	2.01 (1.84 ... 2.17)	-0.201 (-0.272 ... -0.144)	reasonable, include as different experiment than most other models
ACCESS-CM2 historical-ssp585 (2)	good	good	1.86 (1.71 ... 2.02)	-0.200 (-0.260 ... -0.120)	good
AWI-CM-1-1-MR historical-ssp585 (1)	good	good	1.50 (1.35 ... 1.69)	-0.200 (-0.280 ... -0.110)	good
CNRM-CM6-1 historical-ssp585 (1)	good	good	1.54 (1.39 ... 1.72)	-0.210 (-0.290 ... -0.100)	good
CNRM-CM6-1-HR historical-ssp585 (1)	good	good	1.48 (1.33 ... 1.66)	-0.190 (-0.270 ... -0.100)	good
CNRM-ESM2-1 historical-ssp585 (1)	good	good	1.71 (1.54 ... 1.92)	-0.180 (-0.250 ... -0.0900)	good
CanESM5 historical-ssp585 (50)	good	reasonable	1.79 (1.76 ... 1.82)	-0.180 (-0.190 ... -0.170)	reasonable, include because statistical parameters good
EC-Earth3 historical-ssp585 (3)	good	good	1.87 (1.76 ... 2.00)	-0.220 (-0.270 ... -0.170)	good
FGOALS-g3 historical-ssp585 (3)	good	reasonable	1.80 (1.69 ... 1.92)	-0.180 (-0.210 ... -0.140)	reasonable, include because statistical parameters good
GFDL-CM4 historical-ssp585 (1)	good	good	1.43 (1.29 ... 1.62)	-0.210 (-0.300 ... -0.110)	good
INM-CM4-8 historical-ssp585 (1)	good	good	1.63 (1.46 ... 1.83)	-0.210 (-0.300 ... -0.110)	good
INM-CM5-0 historical-ssp585 (1)	good	good	1.80 (1.63 ... 2.03)	-0.240 (-0.310 ... -0.140)	good
IPSL-CM6A-LR historical-ssp585 (6)	good	reasonable	1.79 (1.71 ... 1.88)	-0.220 (-0.250 ... -0.180)	reasonable, include because statistical parameters good
MIROC-ES2L historical-ssp585 (1)	reasonable, peaks early	reasonable	1.46 (1.31 ... 1.65)	-0.190 (-0.300 ... -0.0900)	reasonable, include because statistical parameters good
MPI-ESM1-2-HR historical-ssp585 (2)	good	good	1.49 (1.39 ... 1.62)	-0.250 (-0.310 ... -0.190)	good
MPI-ESM1-2-LR historical-ssp585 (10)	good	good	1.63 (1.58 ... 1.69)	-0.260 (-0.280 ... -0.230)	good
MRI-ESM2-0 historical-ssp585 (2)	reasonable, peak too flat	good	1.41 (1.30 ... 1.53)	-0.280 (-0.340 ... -0.220)	reasonable, include because statistical parameters good
NESM3 historical-ssp585 (1)	good	good	1.48 (1.34 ... 1.67)	-0.290 (-0.370 ... -0.200)	good
NorESM2-MM historical-ssp585 (1)	good	good	1.90 (1.70 ... 2.12)	-0.250 (-0.350 ... -0.140)	in between reasonable and good, include
IPSL-CM6A-LR historical-ssp245 (32)	good, from CMIP6	reasonable, from CMIP6	1.69 (1.64 ... 1.75)	-0.220 (-0.250 ... -0.200)	reasonable, observed GMST used, include
CAM5-1-1degree C20C historical (99)	NA	NA	1.70 (1.68 ... 1.72)	-0.176 (-0.172 ... -0.180)	good, values used with warming level 1.7
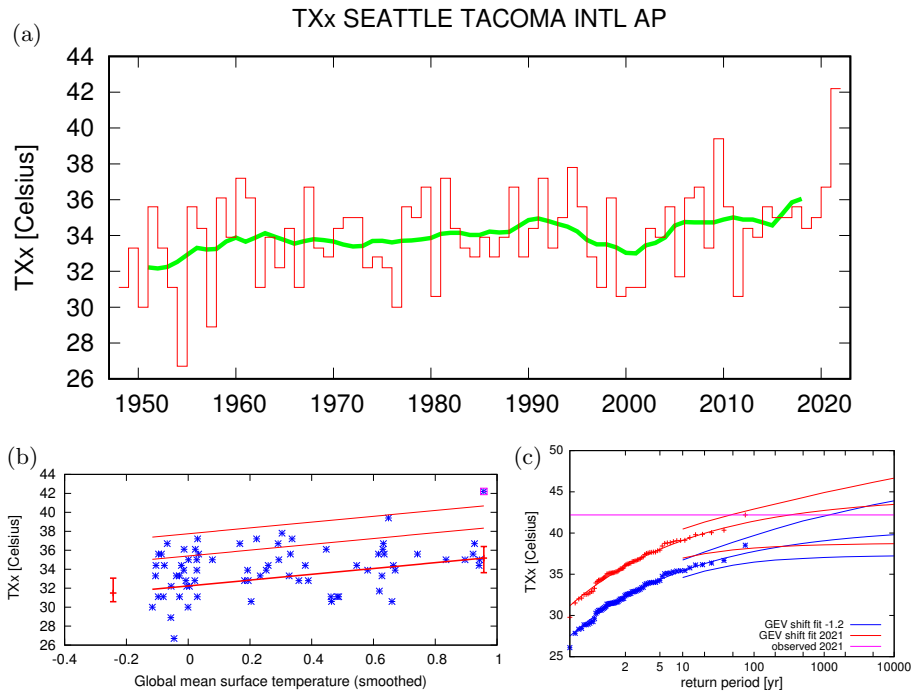
Figure 10. as Figure 9 but for the station data at Seattle-Tacoma International Airport.

to the past (pre-industrial conditions) and, when available, for a climate at +2°C of global warming above pre-industrial climate compared with current climate. The results are visualized in Section 5.

5 Hazard synthesis

250 In Sections 3 and 4 we calculated the probability ratio as well as the change in magnitude of the event in the observations and the models. In this section we combine these results to give an overarching synthesized attribution statement (please see e.g. Kew et al. (2021) for details on the synthesis technique including how weighting is calculated for observations and for models). Observations and models are combined into a single result in two ways. Firstly, we neglect common model uncertainties beyond the averaged model spread that is depicted by the bright red bar, and compute the weighted average of models and observations:

255 this is indicated by the magenta bar, see Figure 12. The weighting applied is the inverse square of the uncertainty (the width of the bright bars). As, due to common model uncertainties, model uncertainty can be larger than the model spread, secondly, we also show the more conservative estimate of an unweighted average of observations and models, indicated by the white box accompanying the magenta bar in the synthesis figures.

Figure 12 shows the synthesis results for the current vs. past climate; the results for the future vs. current climate are

260 presented in Figure 13. Where the results for the probability ratio do not give a finite number we replace them by 10000, to allow all models to be included in the synthesis analysis. This means that the reported synthesized probability ratio gives a more

Table 2. Analysis results showing the model threshold for a 1-in-1000 year event in the current climate, and the probability ratios and intensity changes for the present climate with respect to the past (labelled "past") and for the +2°C GMST future climate with respect to the present (labelled "future").

Model / Observations (number of members)	Threshold	Probability ratio PR - past [-]	Change in intensity ΔT - past [°C]	Probability ratio PR - future [-]	Change in intensity ΔT - future [°C]
ERA5	39.7 °C	3.5e+2 (3.2 ... ∞)	3.1 (1.1 ... 4.7)		
GFDL-CM2.5/FLOR historical-rcp45 (5)	34 °C	6.5e+2 (16 ... ∞)	1.6 (1.2 ... 2.1)	4.6 (3.4 ... 12)	1.2 (1.0 ... 1.3)
ACCESS-CM2 historical-ssp585 (2)	35 °C	25 (2.3 ... ∞)	1.1 (0.41 ... 1.9)	45 (4.5 ... ∞)	1.2 (0.96 ... 1.4)
AWI-CM-1-1-MR historical-ssp585 (1)	36 °C	1.1e+4 (6.6 ... ∞)	1.6 (0.84 ... 2.3)	2.8e+2 (5.5 ... ∞)	1.3 (1.1 ... 1.6)
CNRM-CM6-1 historical-ssp585 (1)	34 °C	1.9 (0.0 ... ∞)	0.22 (-0.51 ... 0.95)	69 (3.4 ... ∞)	1.1 (0.76 ... 1.3)
CNRM-CM6-1-HR historical-ssp585 (1)	35 °C	5.2e+2 (5.4 ... ∞)	1.5 (0.73 ... 2.2)	56 (4.1 ... ∞)	1.3 (1.0 ... 1.5)
CNRM-ESM2-1 historical-ssp585 (1)	38 °C	1.5e+2 (3.6 ... ∞)	1.6 (0.68 ... 2.6)	15 (2.8 ... ∞)	0.97 (0.64 ... 1.3)
CanESM5 historical-ssp585 (50)	38 °C	1.6e+3 (2.6e+2 ... 6.7e+4)	2.0 (1.9 ... 2.1)	62 (32 ... 1.5e+2)	1.5 (1.4 ... 1.5)
EC-Earth3 historical-ssp585 (3)	38 °C	3.2e+2 (8.2 ... ∞)	1.3 (0.88 ... 1.7)	20 (5.2 ... 5.8e+2)	1.2 (1.1 ... 1.4)
FGOALS-g3 historical-ssp585 (3)	41 °C	71 (8.5 ... 2.1e+8)	1.5 (1.0 ... 2.0)	17 (5.2 ... 2.2e+2)	1.1 (0.87 ... 1.3)
GFDL-CM4 historical-ssp585 (1)	31 °C	∞ (14 ... ∞)	2.1 (1.3 ... 3.0)	∞ (16 ... ∞)	1.7 (1.4 ... 1.9)
INM-CM4-8 historical-ssp585 (1)	42 °C	∞ (28 ... ∞)	2.6 (1.7 ... 3.6)	2.7e+3 (6.5 ... ∞)	1.7 (1.4 ... 2.0)
INM-CM5-0 historical-ssp585 (1)	41 °C	∞ (14 ... ∞)	2.2 (0.95 ... 3.3)	∞ (12 ... ∞)	1.6 (1.3 ... 2.0)
IPSL-CM6A-LR historical-ssp585 (6)	34 °C	1.5e+5 (50 ... ∞)	1.7 (1.4 ... 2.0)	2.4e+2 (16 ... ∞)	1.3 (1.1 ... 1.4)
MIROC-ES2L historical-ssp585 (1)	33 °C	75 (1.3 ... ∞)	1.2 (0.040 ... 2.3)	12 (2.2 ... ∞)	0.71 (0.41 ... 1.0)
MPI-ESM1-2-HR historical-ssp585 (2)	34 °C	∞ (27 ... ∞)	1.4 (0.82 ... 1.9)	4.8e+4 (12 ... ∞)	1.2 (0.96 ... 1.4)
MPI-ESM1-2-LR historical-ssp585 (10)	32 °C	∞ (1.1e+11 ... ∞)	1.6 (1.4 ... 1.9)	∞ (1.8e+3 ... ∞)	1.3 (1.2 ... 1.4)
MRI-ESM2-0 historical-ssp585 (2)	32 °C	∞ (1.3e+2 ... ∞)	1.4 (0.86 ... 1.9)	13 (4.9 ... 54)	1.0 (0.84 ... 1.2)
NESM3 historical-ssp585 (1)	30 °C	∞ (1.1e+5 ... ∞)	2.5 (1.9 ... 3.2)	∞ (66 ... ∞)	1.5 (1.3 ... 1.7)
NorESM2-MM historical-ssp585 (1)	41 °C	∞ (11 ... ∞)	2.6 (1.3 ... 3.9)	4.3e+7 (7.0 ... ∞)	1.7 (1.3 ... 2.1)
IPSL-CM6A-LR historical-ssp585 (32)	34 °C	∞ (∞ ... ∞)	2.6 (2.4 ... 2.9)	-	-
CAM5-1-1degree C20C historical (99)	43 °C	2.4e+2 (1.5e+2 ... 3.8e+2)	1.6 (1.5 ... 1.8)	-	-
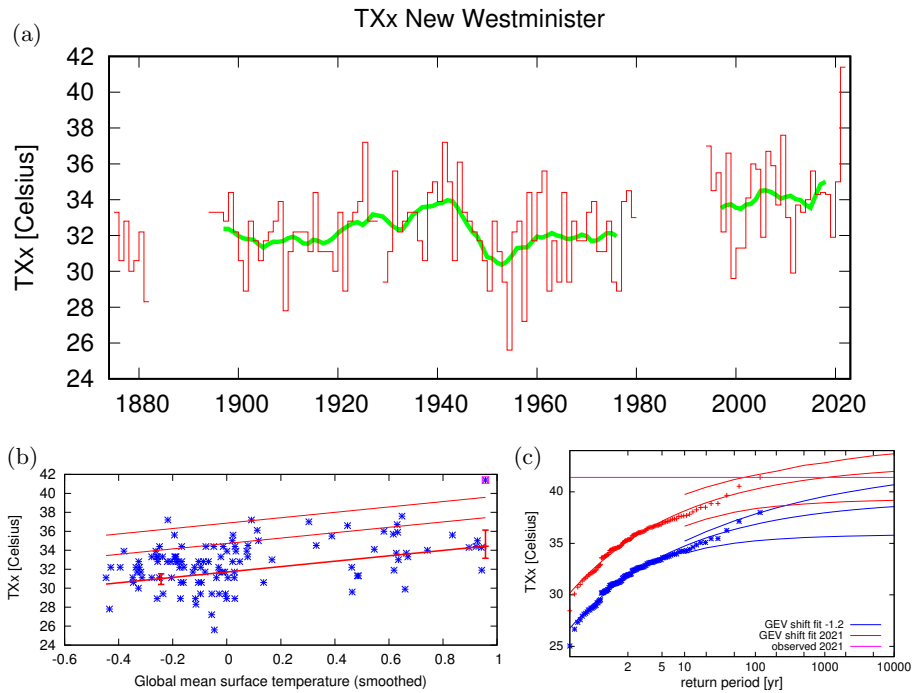
Figure 11. as Figure 9 but for the station data at New Westminster. Source: see text.

conservative, lower value. For the intensity change we report the weighted synthesis value. For probability ratio we can only give a lower estimate of the range. Generally, we do not see any consistent departures in the model results that can be traced back to experiment differences, except that models which consist of many ensemble members have smaller uncertainties.

265   Results for current vs past climate, i.e., for 1.2°C of global warming vs pre-industrial conditions (1850-1900), indicate an increase in intensity of about 2.0 °C (1.2 °C to 2.8 °C) and a PR of at least 150. Model results for additional future changes if global warming reaches 2°C indicate a further increase in intensity of about 1.3 °C (0.8 °C to 1.7 °C) and a PR of at least 3, with a best estimate of 175. This means that an event like the current one, analysed here as having a return period in the current climate of 1000 years, would occur in the future world with 2°C of global warming roughly every 5 to 10 years according to

270   the best PR estimate, albeit with large uncertainties around it. Such a 2°C climate could, according to the IPCC AR6 SSP2-4.5 which is the scenario closest to current emission levels, be reached as early as the 2040s (Lee et al., 2021).

6   The broader context of the heatwave

In the previous section we summarised and synthesised trends in TXx that were detected in observations and attributed to climate change using model data. In this section we provide context to the analysed heat event by evaluating the assumption

275   that this heatwave occurred in this location by chance and by discussing factors that possibly influenced the extremity of this heatwave event, being the specific meteorological conditions and dynamics, preceding dryness - which can amplify temperature
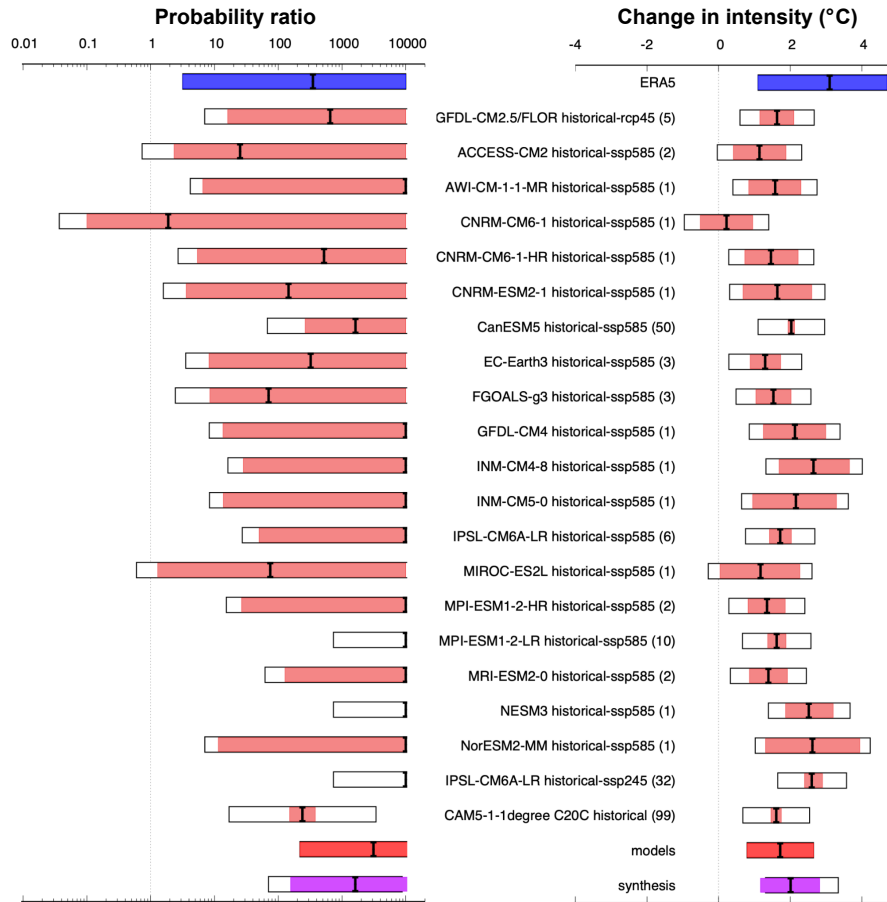
Figure 12. Synthesis of the past climate, showing probability ratios (left) and changes in intensity in °C (right), comparing the 2021 event with a pre-industrial climate. The blue bars show ERA5 results, the light red bars the model results, with common model uncertainty shown as white bars around them. The model average is shown by the bright red bars. The magenta bars are the synthesized values, and the white box accompanying the magenta bar indicates the more conservative estimate of an unweighted average of observations and models. Model names include the model experiment and scenario and the number of ensemble members in brackets.

during heatwaves and reduce evaporation, and the ENSO and PDO modes of of natural variability that are relevant for this region.

6.1 Probability of a chance event

280 In Section 3 we offered two explanations for having such a record breaking heat wave as studied here; it could either occur by chance or nonlinear effects could have made such a heatwave possible. Here we provide some context to the first option by providing an estimate of how many heat waves that are characterised by a return time of 1000 years at their given location
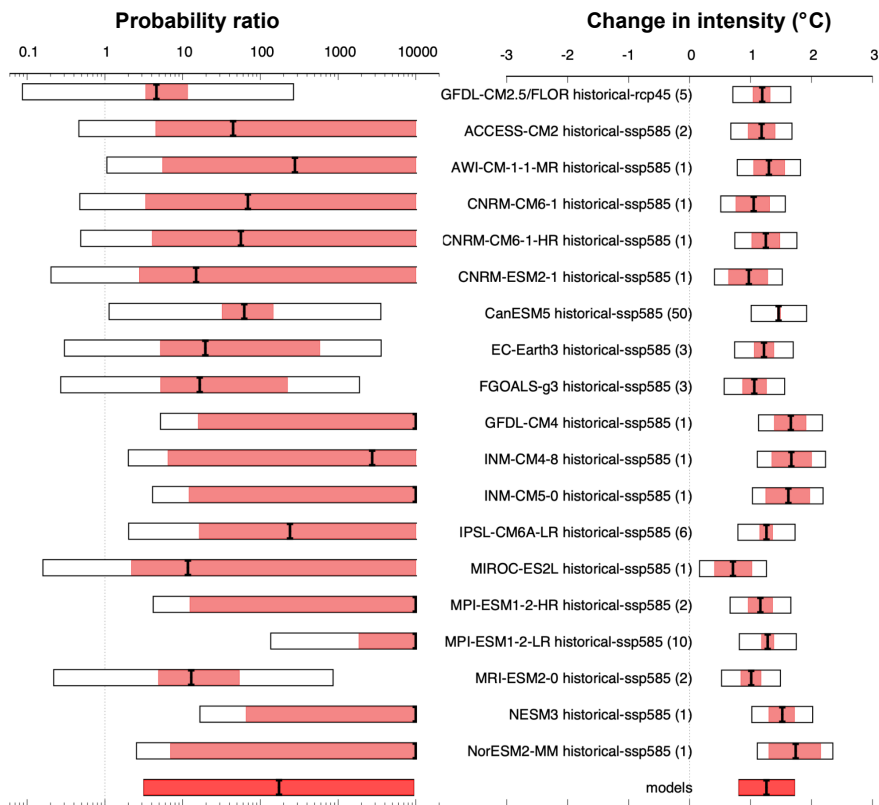
Figure 13. Same as Figure 12 but comparing 2°C of global warming (above pre-industrial) with present-day values (models only).

we can expect on the entire globe. In this study our analysis focuses on the area 45°N-52°N, 119°W-123°W which has been strongly affected by the heatwave. However, the entire area affected by heat is larger - about 1500km x 1500km which is about 1.5% of the land area of the world. Assuming that the event occurred just by chance, we can roughly estimate the global return time, i.e. the worldwide interval at which we would expect a heatwave similar to the one observed in terms of spatial extent and probability to occur at the given location. On the global land masses there are about $1/(1.5\%) \sim 60$ independent areas in which a heatwave of similar spatial resolution could have occurred. This implies that the return time of an event as rare as the Pacific northwest heatwave or rarer, to occur somewhere over land, is about 60 times smaller than the estimated 1000 years interval for such an event to occur at the specific location. This gives a very rough estimate of a return period around 15 years with a lower bound of 1.5 years (not shown) to experience such a heatwave somewhere on the land of the earth. A heatwave of this extent and extremity might therefore no longer be considered very rare if it could be expected anywhere around the globe in one or two decades. Further research on this and other exceptional heatwaves is needed to determine whether this estimate is indeed realistic, i.e., whether or not we should reject the assumption that this heatwave occurred by chance at this location.
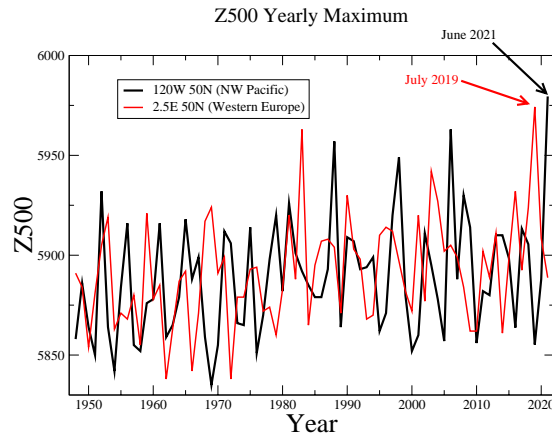
Figure 14. Annual maximum 500 hPa height (m) for two points at the same latitude in two continents. Black: Pacific NW (as above) and red: Western Europe (2.5E; 50N). Data source: NCEP initialized reanalysis.

6.2 Meteorological analysis and dynamics

The evolution of this event can be explained by a confluence of meso- and synoptic-scale dynamical features, potentially including antecedent low soil moisture conditions and anomalously high column specific humidity that are a hallmarks of extreme heat in western North America (Stewart et al., 2017; Bumbaco et al., 2013). At the synoptic scale, an omega-block developed over the study area beginning at roughly 00UTC on June 25th centred at ∼125 °W, 52 °N, which then slowly progressed eastward over subsequent days. This ridge featured a maximal 500 hpa geopotential height of ∼5980 m, which is unprecedented for this area of western North America for the period from 1948 through to June 2021 at least (Figure 14).

Despite being a record, this extreme high pressure system – a feature sometimes called a "Heat dome" – is not that anomalous given the long-term trend in 500 hPa driven by thermal expansion (Christidis and Stott, 2015). Also, comparing recent heatwaves in the Pacific NW to the extreme heatwave in Western Europe in 2019 (Vautard et al., 2020), the geopotential height reached similar anomalies and has a similar long-term trend (Figure 14).

The circulation pattern itself also appears typical for hot summertime temperature: using analogues of 500 hPa and a pattern correlation metric to compare fields, we find that about 1% of June and July circulation patterns, defined as the 500 hPa geopotential height pattern within [160 °W-110 °W; 35 °N-65 °N] in previous years have an anomaly correlation larger than 0.8 with the 28 June pattern. This degree of correlation is typical among days with this type of blocking pattern during the months of June and July. Roughly one third of June and July geopotential height fields have 1% or fewer analogues with an anomaly correlation larger than 0.8. We also find that this fraction does not change when restricting the analogues search within 3 distinct time periods between 1948 and 2020. We conclude that the 28 June circulation is likely not exceptional, while temperatures associated with it were.
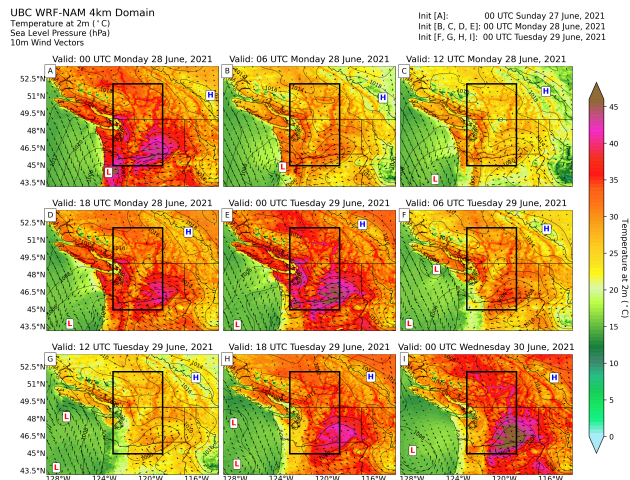
Figure 15. Regional simulation of sea level pressure, 2m air temperature, and 10m wind velocity in the region containing the study area (black box) using the Weather Research and Forecasting (WRF Skamarock et al., 2019) model forced by the North American Mesoscale Forecast System (NAM). Panels (A-I) show the evolution of the near-surface dynamics at a 6-hour interval from 00UTC on the 28th through 00UTC on the 30th of June 2021. Of note is Panel (E) that shows the 5PM local time on the day of peak temperature for Portland, Seattle, and Vancouver.

At the meso-scale, high solar irradiance during the longest days of the year and strong subsidence increased near-surface air temperatures during the event. As is typical for summer heatwaves in the region (Brewer et al., 2012, 2013), a meso-scale thermal trough developed over western Oregon by 00UTC on the 28th June. This feature migrated northward reaching the northern tip of Washington State by 00UTC on the 29th. Further offshore, a small cut-off low travelled southwest to northeast around the synoptic-scale trough that made up the west arm of the omega block. The pressure gradients associated with the thermal trough and the cut-off low promoted moderate E-SE flow in the northern and eastern sectors of the feature and S-SW flow to the south. Near-surface winds with easterly components crossed the Cascade Range of Washington and Oregon and the southern Coast Mountains of British Columbia where they were lighter but sufficient to displace cooler marine air. The difference in elevation on the west and east sides of the mountain ranges contributed to more adiabatic heating than cooling, which helped drive the warmest temperatures observed in the event along the foot of the west slope of these mountains, near or slightly above sea level. These dynamics are illustrated in Figure 15. By 12UTC on the 29th of June 2021, the southwestern portion of the study area was under the influence of southerly to southwesterly near-surface flows that advected marine air and forced marked cooling. Unfortunately, winds associated with this transition intensified a wildfire that quickly consumed the town of Lytton, BC where Canada's nationwide all time high temperature was set just a day before.

There is no scientific consensus whether blocking events are made more severe or persistent because of Arctic amplification or other mechanisms (i.e. Tang et al., 2014; Barnes and Screen, 2015; Vavrus, 2018). We contend that Arctic sea-ice was unlikely to have played a large role in this event largely due to the timing. In early summer, Arctic sea ice remains extensive,
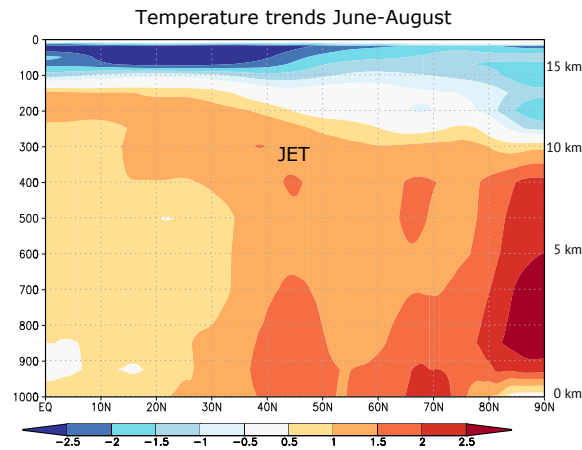
Figure 16. Zonal mean trends in temperature (°C per degree global warming) as function of pressure (hPa) in the ERA5 reanalysis 1979–2019 in the northern hemisphere.

but is melting thus keeping near surface temperatures near 0 °C. This causes summer trends in near-surface temperatures over the Arctic ocean to be smaller than for the midlatitudes. During the months prior to the event, the sea ice extent was below the 1981-2010 mean, but was similar to values observed from 2011 to 2020 (Fetterer et al., 2017 (updated daily). Instead, Arctic Amplification in summer is characterized by strong warming over high-latitude land areas (as can clearly be seen in Figure 335   16) and this warming signal reaches into the upper-troposphere. This enhanced warming is likely related to strong downward trends in early summer snow cover. There is evidence, from observations (Coumou et al., 2015; Chang et al., 2016), climate models (Harvey et al., 2020; Lehmann et al., 2014) and paleo-proxies (Routson et al., 2019), that this enhanced warming over high latitudes leads to a weakening of the jet and storm tracks in summer. This weakening could favour more persistent weather conditions (Pfleiderer et al., 2019; Kornhuber and Tamarin-Brodsky, 2021). Regional-scale interactions between loss of snow 340   cover and low soil moisture associated with earlier snowmelt and rapid springtime soil moisture drying, may have had an enhanced warming impact into early summer in the Arctic. At mid-atmospheric levels there is some amplification remaining due to the winter season (Figure 16), but at the jet level (∼250 hPa) the usual increase of the thermal gradient due to tropical upper tropospheric warming is advected North by the Hadley circulation (Haarsma et al., 2013). The final effect on the jet stream is therefore a competition between factors enhancing and decreasing the temperature gradient.

345   6.3   Drought

An additional feature of the event is the very dry antecedent conditions that may have contributed to observed extreme temperatures through reduced latent cooling from inhibited evapotranspiration. Low soil moisture conditions can lead to a strong amplification of temperature during heatwaves, including nonlinear effects (Seneviratne et al., 2010; Mueller and Seneviratne, 2012; Hauser et al., 2016; Wehrli et al., 2019). In addition, low spring snow level conditions can also further amplify this feed-
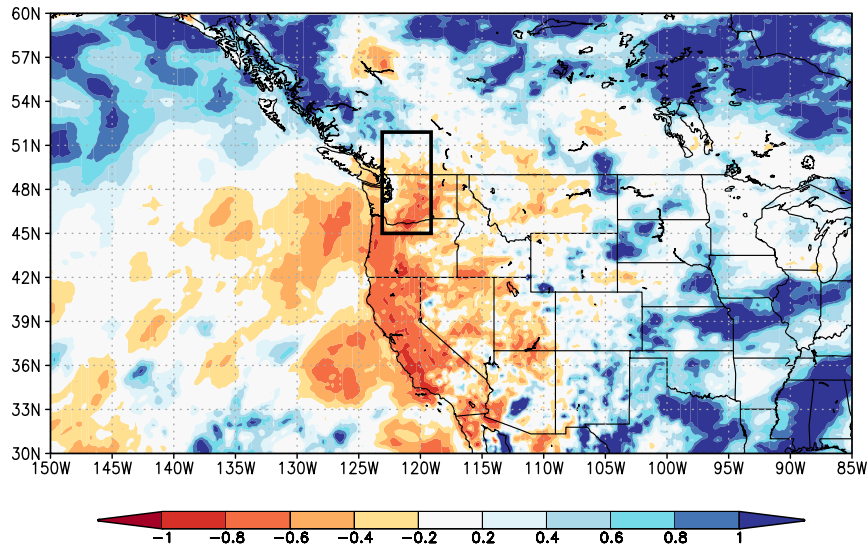
Figure 17. GPM/IMERG satellite estimates of relative precipitation anomalies in March–June 2021 relative to the whole record (2000-2020). The value –1 (dark red) denotes no precipitation, –0.5 (orange) 50% less than normal and zero (light grey) normal precipitation. Origin: KNMI Climate Explorer.

350   back (Hall et al., 2008). In this section we briefly explore whether precipitation anomalies and evapotranspiration measures could have played a role in the extreme heat via feedbacks related to soil moisture conditions.

Integrated Multi-satellitE Retrievals for the Global Precipitation Mission (IMERG) estimates of precipitation during the period from March through June, 2021 indicate anomalously dry conditions from southern BC southward through California (Figure 17). The relative precipitation anomaly ranges from close to zero over the Puget Sound area including Seattle to values 355   of between -0.6 and -0.8, meaning that only 20%-40% of the average amount of precipitation fell in these locations, in Western Oregon. Note that in the northern parts of the area affected by the heatwave, i.e., in the coastal mountains north of Vancouver Island, large positive precipitation anomalies occurred over the months prior to the event.

The available moisture is also influenced by evapotranspiration, which depends strongly on temperature, radiation and available atmospheric moisture. Evaporation in the study area was below normal in the ERA5 reanalysis from March and became 360   more negatively anomalous until May (not shown). During the event in late June, unusual amounts of net radiation counteracted the effects of progressive soil desiccation, and thereby prevented a further decline of evaporation with respect to its climatological expectation.

Satellite-based measurements of surface soil moisture based on microwave remote sensing from the European Space Agency (ESA) Climate Change Initiative (CCI) provided by the Copernicus service suggest that surface soil moisture was below

normal in the region since the beginning of April and that the anomalous conditions persisted until June (https://dataviewer. geo.tuwien.ac.at/?state=88bf0c), in agreement with the decreased precipitation and somewhat below normal evapotranspiration in the ERA5 reanalysis.

6.4 Influence of modes of natural variability

The El Niño Southern Oscillation is the dominant source of interannual variability in the region through the Pacific North American teleconnection. The influence is typically greatest in late winter and spring and has less clear impacts during summer and fall. Because ENSO was neutral during the preceding months and the impacts on TXx are minimal (r<0.1) we conclude that it had no influence on the occurrence of the heatwave.

The Pacific Decadal Oscillation (PDO) can affect some aspects of North American summer weather, although again the connections to heatwaves in this region are very weak. The strongly negative values of the PDO index, as they occurred in May, would slightly favor cooler conditions for this region. PDO thus also is unlikely to have played an important role in the event.

Altogether, external modes of variability appear to have played little to no role in the formation of the event.

7 Vulnerability and exposure

The Pacific Northwest region is not accustomed to very hot temperatures such as those experienced during the June 2021 heatwave. Heatwaves are one of the deadliest natural hazards, resulting in high excess mortality through direct impacts of heat (e.g. heat stroke) and by exacerbating pre-existing medical conditions linked to respiratory and cardiovascular issues (Haines et al., 2006; Ebi et al., 2021). In addition to more than 1,000 excess heat-related deaths, there was a significant increase in emergency department visits.[23] On June 28, 2021 alone, there were 1,038 heat-related emergency department visits in the U.S. Department of Health and Human Services Region that includes Alaska, Idaho. Oregon, and Washington, compared with nine visits on the same date in 2019.[4] The mean daily number of heat-related illness emergency department visits in the region for 25-30 June 2021(424) was 69-times higher than during the same days in 2019 (6). Although this region covers about 4% of the US population, it accounted for about 15% of all heat-related illness emergency department visits nationwide during June.

The June 2021 heatwave also affected critical infrastructure such as roads and rail and caused power outages, agricultural impacts, and forced many businesses and schools to close.[5][6] Rapid snowmelt in BC caused water levels to rise, leading to evacuation orders north of Vancouver.[7] Furthermore, in some places, wildfires, the risk of which has increased due to climate

---

[2]https://www.nytimes.com/interactive/2021/08/11/climate/deaths-pacific-northwest-heat-wave.html

[3]https://www.cbc.ca/news/canada/british-columbia/bc-heat-dome-sudden-deaths-570-1.6122316

[4]https://www.cdc.gov/mmwr/volumes/70/wr/mm7029e1.htm

[5]https://apnews.com/article/canada-heat-waves-environment-and-nature-cc9d346d495caf2e245fc9ae923adae1

[6]https://www.seattletimes.com/seattle-news/weather/pacific-northwests-record-smashing-heat-wave-primes-wildfire-buckles-roads-health-toll-not-yet-known

[7]https://globalnews.ca/news/7994540/flooding-record-breaking-heat-rapid-snow-melt-bc-video/

change in this region (Kirchmeier-Young et al., 2019), started and quickly spread, requiring entire towns to evacuate.[8] The co-occurence of such events may result in compound risks, for example as households are advised to shut windows to keep outdoor wildfire smoke from getting inside, while simultaneously threatened by high indoor temperatures when lacking air conditioning.

395   Timely warnings were issued throughout the region by the US National Weather Service, Environment and Climate Change Canada, and local governments. British Columbia has a "Municipal Heat Response Planning" summary review that gathers information on heat response plans throughout the province, including responses such as increasing access to cooling facilities and distribution of drinking water. In long-term strategies, changes to the built environment are emphasized (Lubik et al., 2017). Not all municipalities throughout the Pacific Northwest and BC have formalized heat response plans, and others have limited

400 planning, thought to be due to low heat risk perceptions throughout the area, as well as a lack of local data for risk assessments (Lubik et al., 2017).

     The extremely high temperatures that occurred in this heat episode meant that everyone was vulnerable to its effects if exposed for a long enough period of time. Although extreme heat affects everyone, some individuals are more vulnerable, including the elderly, young children, individuals with pre-existing medical conditions, socially isolated individuals, homeless

405 people, individuals without air-conditioning, and (outdoor) workers (Singh et al., 2019). Seattle's King County contains the third-largest population of homeless people in the U.S, with the numbers increasing during the past decade (Stringfellow and Wagle, 2018). Governmental authorities opened cooling centres throughout Seattle, Portland, and Vancouver BC during the June 2021 heatwave. [9] [10] [11] Further, electrolytes, food, and water were distributed to homeless people. [12]

     The lack of air conditioning contributes to heat risk. The Pacific Northwest has lower access to air-conditioned homes and

410 buildings compared to other regions in the U.S., with the Seattle metropolitan area being the least air-conditioned metropolitan area of the United States (<50% air conditioning in residential areas) (U.S. Census Bureau). Portland and Vancouver also have low percentages of air-conditioned households, 79% and 39% respectively (BC Hydro; U.S. Census Bureau). An increasing trend in air conditioned homes is occurring in all three cities (ibid.).

8   Conclusions and recommendations

415 In this study, the influence of human-induced climate change on the intensity and probability of the Pacific Northwest heatwave of 2021 was investigated. We analysed how the annual maxima of daily maximum temperatures are changing with increasing global mean surface temperature, studying the area 45 °N–52 °N, 119 °W–123 °W that includes the cities Vancouver, Seattle and Portland. Synthesizing results from weather observations and model simulations, we conclude that the occurrence of a heatwave of the intensity experienced in the study area would have been virtually impossible without human-caused climate

---

[8] https://www.washingtonpost.com/world/2021/07/01/lytton-canada-evacuated-wildfire-heatwave/

[9] https://durkan.seattle.gov/2021/06/city-of-seattle-opens-additional-cooling-centers-and-updated-guidance-for-staying-cool-in-extreme-heat%E2%80%AF/

[10] https://www.oregonlive.com/weather/2021/06/portland-cooling-centers-provide-relief-from-heat.html

[11] https://thebcarea.com/2021/06/26/cooling-stations-set-up-around-b-c-for-record-breaking-heat-wave-this-weekend/#comments

[12] https://edition.cnn.com/2021/06/29/weather/northwest-heat-illness-emergency-room/index.html

420 change. Whilst the extremity of this event made it challenging to robustly determine how rare it currently is, this general result is not strongly tied to the exact return period. For this analysis, we defined the probability of the event as one in 1000-yrs in the current climate and found that the event would have been at least 150 times rarer without human-induced climate change. Also, this heatwave was about 2 °C (1.2 °C to 2.8 °C) hotter due to human induced climate change. Looking into the future to a world with 2 °C of global warming, an event like this, currently estimated to occur only once every 1000 years, would occur

425 roughly every 5 to 10 years according to the best PR estimate, albeit with large uncertainties around it.

This record-breaking extreme event has been analysed under the assumption that it was simply a low probability random event. A rudimentary calculation looking into the probability of a random event of this scale and severity to occur anywhere over the earth's land area, gave an estimated chance of order 1-in-15 years, which at first impression makes a random event seem plausible, but this should be more thoroughly investigated.

430 The alternative is that nonlinear interactions and feedbacks occurred, which amplified the intensity of this extreme, placing it in a different population of heatwave events with different (and possibly unknown) statistics. We briefly considered dynamical and hydrological (drought) mechanisms and modes of natural variability that could have had an amplifying role. The conditions in the preceding months were dry but not extremely anomalous. The circulation itself was highly anomalous but not exceptional enough to explain the record breaking heat alone, however, local topography and preceding dryness may have amplified the

435 associated temperatures. In addition, there may also be dynamical mechanisms (Arctic Amplification) at work that influence the persistence of blocking conditions.

Further research is planned to investigate whether these or other feedbacks were operating in this outstanding event, and whether those feedbacks are related to human-induced climate change and if they increase the frequency beyond that expected for random events of such extreme temperatures. Also, further research is needed into the limitations of standard GEV analysis

440 on annual maxima with short records and seemingly non-stationary behavior.

Whether or not local or dynamical feedbacks are responsible for amplifying the extreme temperatures in this particular event, this study shows that the human-induced warming that has occurred since pre-industrial conditions does make extreme events like this possible in the current climate and study region, and many times more likely than in the pre-industrial era.

Adaptation measures therefore need to be much more ambitious and take account of the rising risk of heatwaves around the

445 world. Although this extreme heat event is still rare in today's climate, the analysis above shows that the frequency is increasing with further warming. Deaths from extreme heat can be dramatically reduced with adequate preparedness action – a number of adaptation and risk management priorities emerge. It is crucial that local governments and their emergency management partners establish heat action plans to ensure well coordinated response actions during an extreme heat event - tailored to high-risk groups (Ebi, 2019). Heatwave early warning systems also need to be improved, which includes tailoring messages

450 to inform and motivate vulnerable groups, as well as providing tiered warnings that take into account vulnerable groups may have lower thresholds for risk (Hess and Ebi, 2016). In other words, it is important to start to warn the most vulnerable as temperatures start to rise even though the general population is not yet acutely at risk. In cases where heat action plans and heat early warning systems are already robust, it is important that they are reviewed and updated to capture the implications of rising risks - every five years or less (Hess and Ebi, 2016). Further, heatwave early warning systems should undergo stress tests to

455 evaluate their robustness to temperature extremes beyond recent experience and to identify modifications to ensure continued effectiveness in a changing climate (Ebi et al., 2018).

Data availability. Data are available via the KNMI Climate Explorer (https://climexp.knmi.nl/)

Appendix A: Validation tables

Table A1: As Table 1 but showing all model validation results.

Model / Observations (number of members)	Seasonal cycle	Spatial pattern	Sigma	Shape parameter	Conclusion
ERA5			1.70 (1.40 ... 1.90)	-0.200 (-0.500 ... 0.00)	
GFDL-CM2.5/FLOR historical-rcp45 (5)	good	good	2.01 (1.84 ... 2.17)	-0.201 (-0.272 ... -0.144)	reasonable, include as different experiment than most other models
ACCESS-CM2 historical-ssp585 (2)	good	good	1.86 (1.71 ... 2.02)	-0.200 (-0.260 ... -0.120)	good
ACCESS-ESM1-5 historical-ssp585 (2)	good	good	2.69 (2.49 ... 2.90)	-0.240 (-0.290 ... -0.190)	bad
AWI-CM-1-1-MR historical-ssp585 (1)	good	good	1.50 (1.35 ... 1.69)	-0.200 (-0.280 ... -0.110)	good
BCC-CSM2-MR historical-ssp585 (1)	good	good	2.22 (2.00 ... 2.49)	-0.230 (-0.310 ... -0.140)	bad
CAMS-CSM1-0 historical-ssp585 (1)	good	good	1.98 (1.79 ... 2.23)	-0.200 (-0.290 ... -0.100)	reasonable, exclude because enough good CMIP5 models
CMCC-CM2-SR5 historical-ssp585 (1)	good	good	1.29 (1.15 ... 1.46)	-0.0800 (-0.160 ... 0.0300)	reasonable, exclude because enough good CMIP5 models
CNRM-CM6-1 historical-ssp585 (1)	good	good	1.54 (1.39 ... 1.72)	-0.210 (-0.290 ... -0.100)	good
CNRM-CM6-1-HR historical-ssp585 (1)	good	good	1.48 (1.33 ... 1.66)	-0.190 (-0.270 ... -0.100)	good
CNRM-ESM2-1 historical-ssp585 (1)	good	good	1.71 (1.54 ... 1.92)	-0.180 (-0.250 ... -0.0900)	good
CanESM5 historical-ssp585 (50)	good	reasonable	1.79 (1.76 ... 1.82)	-0.180 (-0.190 ... -0.170)	reasonable, include because statistical parameters good
EC-Earth3 historical-ssp585 (3)	good	good	1.87 (1.76 ... 2.00)	-0.220 (-0.270 ... -0.170)	good
EC-Earth3-Veg historical-ssp585 (4)	good	good	2.07 (1.95 ... 2.19)	-0.250 (-0.290 ... -0.210)	bad
FGOALS-g3 historical-ssp585 (3)	good	reasonable	1.80 (1.69 ... 1.92)	-0.180 (-0.210 ... -0.140)	reasonable, include because statistical parameters good

GFDL-CM4 historical-ssp585 (1)	good	good	1.43 (1.29 ... 1.62)	-0.210 (-0.300 ... -0.110)	good
GFDL-ESM4 historical-ssp585 (1)	good	good	1.37 (1.23 ... 1.55)	-0.170 (-0.260 ... -0.0700)	reasonable, exclude because enough good CMIP5 models
HadGEM3-GC31-LL historical-ssp585 (4)	good	good	2.00 (1.90 ... 2.12)	-0.210 (-0.250 ... -0.170)	reasonable, exclude because enough good CMIP5 models
HadGEM3-GC31-MM historical-ssp585 (3)	good	good	2.08 (1.96 ... 2.22)	-0.190 (-0.230 ... -0.140)	bad
INM-CM4-8 historical-ssp585 (1)	good	good	1.63 (1.46 ... 1.83)	-0.210 (-0.300 ... -0.110)	good
INM-CM5-0 historical-ssp585 (1)	good	good	1.80 (1.63 ... 2.03)	-0.240 (-0.310 ... -0.140)	good
IPSL-CM6A-LR historical-ssp585 (6)	good	reasonable	1.79 (1.71 ... 1.88)	-0.220 (-0.250 ... -0.180)	reasonable, include because statistical parameters good
KACE-1-0-G historical-ssp585 (3)	good	good	2.27 (2.13 ... 2.41)	-0.241 (-0.282 ... -0.196)	bad
MIROC-ES2L historical-ssp585 (1)	reasonable, peaks about a month early	reasonable	1.46 (1.31 ... 1.65)	-0.190 (-0.300 ... -0.0900)	reasonable, include because statistical parameters good
MIROC6 historical-ssp585 (50)	good	good	1.31 (1.29 ... 1.33)	-0.220 (-0.220 ... -0.210)	bad
MPI-ESM1-2-HR historical-ssp585 (2)	good	good	1.49 (1.39 ... 1.62)	-0.250 (-0.310 ... -0.190)	good
MPI-ESM1-2-LR historical-ssp585 (10)	good	good	1.63 (1.58 ... 1.69)	-0.260 (-0.280 ... -0.230)	good
MRI-ESM2-0 historical-ssp585 (2)	reasonable, peak too flat	good	1.41 (1.30 ... 1.53)	-0.280 (-0.340 ... -0.220)	reasonable, include because statistical parameters good
NESM3 historical-ssp585 (1)	good	good	1.48 (1.34 ... 1.67)	-0.290 (-0.370 ... -0.200)	good
NorESM2-MM historical-ssp585 (1)	good	good	1.90 (1.70 ... 2.12)	-0.250 (-0.350 ... -0.140)	in between reasonable and good, include
UKESM1-0-LL historical-ssp585 (5)	good	good	1.99 (1.90 ... 2.09)	-0.170 (-0.190 ... -0.140)	reasonable, exclude because enough good CMIP5 models
IPSL-CM6A-LR historical-ssp245 (32)	good, from CMIP6	reasonable, from CMIP6	1.69 (1.64 ... 1.75)	-0.220 (-0.250 ... -0.200)	reasonable, observed GMST used, include
GFDL-AM2.5C360 historical (5)	good	good	2.15 (1.99 ... 2.30)	-0.259 (-0.335 ... -0.197)	bad, variability too high
CAM5-1-1degree C20C historical (99)	NA	NA	1.70 (1.68 ... 1.72)	-0.176 (-0.172 ... -0.180)	good, values used with warming level 1.7
MIROC5 C20C historical ()	NA	NA	1.36 (1.33 ... 1.39)	-0.240 (-0.224 ... -0.256)	bad

HadGEM3-A-N216 C20C historical ()	NA	NA	2.00 (1.95 ... 2.05)	-0.240 (-0.218 ... -0.262)	bad

Author contributions. SYP and SFK are the study co-leads, GJvO, FSA, SIS, RV, DC, KLE, JA, RS, MvA and CPM provided analyses and text, MW, WY, SL, DLS, MH, RB and LNL provided data and the synthesis, FL, NG, JT and GAV improved the text, CR, RBS and RH provided figures and FELO initiated the study and contributed to the discussions.

Competing interests. The authors declare no competing interest.

Acknowledgements. We acknowledge the World Climate Research Programme, which, through its Working Group on Coupled Modelling, coordinated and promoted CMIP6. We thank the climate modeling groups for producing and making available their model output, the Earth System Grid Federation (ESGF) for archiving the data and providing access, and the multiple funding agencies who support CMIP6 and ESGF. We thank Urs Beyerle for downloading and curating the CMIP6 data at ETH Zurich. F.L. was supported by the Regional and Global Model Analysis (RGMA) component of the Earth and Environmental System Modeling Program of the U.S. Department of Energy's Office of Biological & Environmental Research (BER) via National Science Foundation IA 1947282.

We would like to express our deep gratitude and respect to Geert Jan van Oldenborgh, co-author of this manuscript, who sadly passed away on 12th October 2021. His outstanding contribution to the science of extreme event attribution and his passion to provide the knowledge, data and analysis tools (https://climexp.knmi.nl/) that are most relevant for society and especially for vulnerable communities has been enormous. We lost an incredible scientist, passionate colleague, and friend.

References

Baldwin, J. W., Dessy, J. B., Vecchi, G. A., and Oppenheimer, M.: Temporally Compound Heat Wave Events and Global Warming: An Emerging Hazard, Earth's Future, 7, 411–427, https://doi.org/https://doi.org/10.1029/2018EF000989, 2019.

Barnes, E. A. and Screen, J. A.: The impact of Arctic warming on the midlatitude jet-stream: Can it? Has it? Will it?, Wiley Interdisciplinary Reviews: Climate Change, 6, 277–286, https://doi.org/10.1002/wcc.337, 2015.

BC Hydro: Not-so well-conditioned: How inefficient A/C use is leaving British Columbians out of pocket in the cold, https://www.google.com/url?q=https://www.bchydro.com/content/dam/BCHydro/customer-portal/documents/news-and-features/ bch-ac-report-aug-2020.pdf&sa=D&source=editors&ust=1631004798219000&usg=AOvVaw2Tf3ZD61NG2ahqg_dm7a-k, 2020.

Boucher, O., Servonnat, J., Albright, A. L., Aumont, O., Y., B., Bastriko, V., Bekki, S., Bonnet, R., Bony, S., Bopp, L., Braconnot, P., Brockmann, P., Cadule, P., Caubel, A., Cheru, F., Cozic, A., Cugnet, D., D'Andrea, F., Davini, P., de Lavergne, C., Denvil, S., Deshayes, J., M., D., Ducharne, A., Dufresne, J.-L., Dupont, E., Ethé, C., Fairhead, L., Falletti, L., Foujols, M.-A., Gardoll, S., Gastinea, G., J., G., Grandpeix, J.-Y., Guenet, B., Guez, L., Guilyardi, E., Guimberteau, M., Hauglustaine, D., Hourdin, F., Idelkadi, A., Joussaume, S., Kageyama, M., Khadre-Traoré, A., Khodri, M., Krinner, G., Lebas, N., Levavasseur, G., Lévy, C., Li, L., Lott, F., Lurton, T., Luyssaert, S., G., M., Madeleine, J.-B., Maignan, F., Marchand, M., Marti, O., Mellul, L., Meurdesoif, Y., Mignot, J., Musat, I., Ottlé, C., Peylin, P., Planton, Y., Polcher, J., Rio, C., Rousset, C., Sepulchre, P., Sima, A., Swingedouw, D., Thieblemont, R., Traoré, A., Vancoppenolle, M., Vial, J., Vialard, J., Viovy, N., and Vuichard, N.: Presentation and evaluation of the IPSL-CM6A-LR climate model, J. Adv. Modeling Earth Systems, 12, e2019MS002 010, https://doi.org/10.1029/2019MS002010, 2020.

Brewer, M. C., Mass, C. F., and Potter, B. E.: The West Coast Thermal Trough: Climatology and Synoptic Evolution, Monthly Weather Review, 140, 3820 – 3843, https://doi.org/10.1175/MWR-D-12-00078.1, 2012.

Brewer, M. C., Mass, C. F., and Potter, B. E.: The West Coast Thermal Trough: Mesoscale Evolution and Sensitivity to Terrain and Surface Fluxes, Monthly Weather Review, 141, 2869 – 2896, https://doi.org/10.1175/MWR-D-12-00305.1, 2013.

Bumbaco, K. A., Dello, K. D., and Bond, N. A.: History of Pacific Northwest Heat Waves: Synoptic Pattern and Trends, Journal of Applied Meteorology and Climatology, 52, 1618 – 1631, https://doi.org/10.1175/JAMC-D-12-094.1, 2013.

Chan, D., Vecchi, G., Yang, W., and Huybers, P.: Improved simulation of 19th-and 20th-century North Atlantic hurricane frequency after correcting historical sea surface temperatures, Science advances, 7, https://doi.org/10.1126/sciadv.abg6931, publisher Copyright: © 2021 American Association for the Advancement of Science. All rights reserved., 2021.

Chang, E. K. M., Ma, C.-G., Zheng, C., and Yau, A. M. W.: Observed and projected decrease in Northern Hemisphere extra-tropical cyclone activity in summer and its impacts on maximum temperature, Geophysical Research Letters, 43, 2200–2208, https://doi.org/https://doi.org/10.1002/2016GL068172, 2016.

Christidis, N. and Stott, P. A.: Changes in the geopotential height at 500?hPa under the influence of external climatic forcings, Geophysical Research Letters, 42, 10,798–10,806, https://doi.org/https://doi.org/10.1002/2015GL066669, 2015.

Ciavarella, A., Cotterill, D., Stott, P., Kew, S., Philip, S., van Oldenborgh, G. J., Skålevåg, A., Lorenz, P., Robin, Y., Otto, F., Hauser, M., Seneviratne, S. I., Lehner, F., and Zolina, O.: Prolonged Siberian heat of 2020 almost impossible without human influence, Climatic Change, 166, 9, https://doi.org/10.1007/s10584-021-03052-w, 2021.

Coumou, D., Lehmann, J., and Beckmann, J.: Climate change. The weakening summer circulation in the Northern Hemisphere mid-latitudes, Science (New York, N.Y.), 348, https://doi.org/10.1126/science.1261768, 2015.

Cowan, T., Hegerl, G. C., Schurer, A., Tett, S. F. B., Vautard, R., Yiou, P., Jézéquel, A., Otto, F. E. L., Harrington, L. J., and Ng, B.: Ocean and land forcing of the record-breaking Dust Bowl heatwaves across central United States, Nature Communications, 11, 2870, https://doi.org/10.1038/s41467-020-16676-w, 2020.

D'Ippoliti, D., Michelozzi, P., Marino, C., de'Donato, F., Menne, B., Katsouyanni, K., Kirchmayer, U., Analitis, A., Medina-Ramón, M., Paldy, A., Atkinson, R., Kovats, S., Bisanti, L., Schneider, A., Lefranc, A., Iñiguez, C., and Perucci, C. A.: The impact of heat waves on mortality in 9 European cities: results from the EuroHEAT project, Environmental Health, 9, 37, https://doi.org/10.1186/1476-069X-9-37, 2010.

Donat, M. G., King, A. D., Overpeck, J. T., Alexander, L. V., Durre, I., and Karoly, D. J.: Extraordinary heat during the 1930s US Dust Bowl and associated large-scale conditions, Climate Dynamics, 46, 413–426, https://doi.org/10.1007/s00382-015-2590-5, 2016.

Donat, M. G., Pitman, A. J., and Seneviratne, S. I.: Regional warming of hot extremes accelerated by surface energy fluxes, Geophys. Res. Lett., 44, 7011–7019, https://doi.org/10.1002/2017GL073733, 2017.

Ebi, K. L.: Effective heat action plans: research to interventions, Environmental Research Letters, 14, 122 001, https://doi.org/10.1088/1748-9326/ab5ab0, 2019.

Ebi, K. L., Berry, P., Hayes, K., Boyer, C., Sellers, S., Enright, P. M., and Hess, J. J.: Stress Testing the Capacity of Health Systems to Manage Climate Change-Related Shocks and Stresses, International Journal of Environmental Research and Public Health, 15, https://doi.org/10.3390/ijerph15112370, 2018.

Ebi, K. L., Capon, A., Berry, P., Broderick, C., de Dear, R., Havenith, G., Honda, Y., Kovats, R. S., Ma, W., Malik, A., Morris, N. B., Nybo, L., Seneviratne, S. I., Vanos, J., and Jay, O.: Hot weather and heat extremes: health risks, The Lancet, 398, 698–708, https://doi.org/10.1016/S0140-6736(21)01208-3, 2021.

Eyring, V., Bony, S., Meehl, G. A., Senior, C. A., Stevens, B., Stouffer, R. J., and Taylor, K. E.: Overview of the Coupled Model Intercomparison Project Phase 6 (CMIP6) experimental design and organization, Geoscientific Model Development, 9, 1937–1958, https://doi.org/10.5194/gmd-9-1937-2016, 2016.

Fetterer, F., Knowles, K., Meier, W. N., Savoie, M., and Windnagel, A. K.: Sea Ice Index, Version 3. Ice Extent; Sea Ice Concentration, https://doi.org/10.7265/N5K072F8, accessed 2 July 2021, 2017 (updated daily).

Haarsma, R. J., Selten, F., and van Oldenborgh, G. J.: Anthropogenic changes of the thermal and zonal flow structure over Western Europe and Eastern North Atlantic in CMIP3 and CMIP5 models, Clim. Dyn., 41, 2577–2588, https://doi.org/10.1007/s00382-013-1734-8, 2013.

Haines, A., Kovats, R. S., Campbell-Lendrum, D., and Corvalan, C.: Climate change and human health: impacts, vulnerability, and mitigation., Lancet, 367, 2101–2109, https://doi.org/10.1016/S0140-6736(06)68933-2, erratum in Lancet. 2006 Aug 19;368(9536):646, 2006.

Hall, A., Qu, X., and Neelin, J. D.: Improving predictions of summer climate change in the United States, Geophysical Research Letters, 35, https://doi.org/https://doi.org/10.1029/2007GL032012, 2008.

Hansen, J., Ruedy, R., Sato, M., and Lo, K.: Global Surface Temperature Change, Rev. Geophys., 48, RG4004, https://doi.org/DOI 10.1029/2010RG000345, 2010.

Harvey, B. J., Cook, P., Shaffrey, L. C., and Schiemann, R.: The Response of the Northern Hemisphere Storm Tracks and Jet Streams to Climate Change in the CMIP3, CMIP5, and CMIP6 Climate Models, Journal of Geophysical Research: Atmospheres, 125, e2020JD032 701, https://doi.org/https://doi.org/10.1029/2020JD032701, e2020JD032701 2020JD032701, 2020.

Hauser, M., Orth, R., and Seneviratne, S. I.: Role of soil moisture versus recent climate change for the 2010 heat wave in western Russia, Geophysical Research Letters, 43, 2819–2826, https://doi.org/https://doi.org/10.1002/2016GL068036, 2016.

Henderson, S. B., McLean, Kathleen E. andLee, M., and Kosatsky, T.: Extreme heat events are public health emergencies, BC Medical Journal, 63, 366–367, 2021.

Hersbach, H., Bell, W., Berrisford, P., Horányi, A., J., M.-S., Nicolas, J., Radu, R., Schepers, D., Simmons, A., Soci, C., and Dee, D.: Global reanalysis: goodbye ERA-Interim, hello ERA5, ECMWF Newsletter, 159, 17–24, https://doi.org/10.21957/vf291hehd7, 2019.

550 Hess, J. J. and Ebi, K. L.: Iterative management of heat early warning systems in a changing climate, Annals of the New York Academy of Sciences, 1382, 21–30, https://doi.org/https://doi.org/10.1111/nyas.13258, 2016.

Kew, S. F., Philip, S. Y., Hauser, M., Hobbins, M., Wanders, N., van Oldenborgh, G. J., van der Wiel, K., Veldkamp, T. I. E., Kimutai, J., Funk, C., and Otto, F. E. L.: Impact of precipitation and increasing temperatures on drought trends in eastern Africa, Earth System Dynamics, 12, 17–35, https://doi.org/10.5194/esd-12-17-2021, 2021.

555 Kirchmeier-Young, M. C., Gillett, N. P., Zwiers, F. W., Cannon, A. J., and Anslow, F. S.: Attribution of the Influence of Human-Induced Climate Change on an Extreme Fire Season, Earth's Future, 7, 2–10, https://doi.org/https://doi.org/10.1029/2018EF001050, 2019.

Kornhuber, K. and Tamarin-Brodsky, T.: Future Changes in Northern Hemisphere Summer Weather Persistence Linked to Projected Arctic Warming, Geophysical Research Letters, 48, e2020GL091 603, https://doi.org/https://doi.org/10.1029/2020GL091603, e2020GL091603 2020GL091603, 2021.

560 Lee, J.-Y., Marotzke, J., Bala, G., Cao, L., Corti, S., Dunne, J., Engelbrecht, F., Fischer, E., Fyfe, J., Jones, C., Maycock, A., Mutemi, J., Ndiaye, O., Panickal, S., and Zhou, T.: Future Global Climate: Scenario-Based Projections and Near-Term Information, in: Climate Change 2021: The Physical Science Basis. Contribution of Working Group I to the Sixth Assessment Report of the Intergovernmental Panel on Climate Change, edited by Masson-Delmotte, V., Zhai, P., Pirani, A., Connors, S., Péan, C., Berger, S., Caud, N., Chen, Y., Goldfarb, L., Gomis, M., Huang, M., Leitzell, K., Lonnoy, E., Matthews, J., Maycock, T., Waterfield, T., Yelekçi, O., Yu, R., and B., Z., 565 chap. 4, Cambridge University Press, in press, 2021.

Lehmann, J., Coumou, D., Frieler, K., Eliseev, A. V., and Levermann, A.: Future changes in extratropical storm tracks and baroclinicity under climate change, Environmental Research Letters, 9, 084 002, https://doi.org/10.1088/1748-9326/9/8/084002, 2014.

Lenssen, N. J. L., Schmidt, G. A., Hansen, J. E., Menne, M. J., Persin, A., Ruedy, R., and Zyss, D.: Improvements in the GISTEMP Uncertainty Model, Journal of Geophysical Research: Atmospheres, 124, 6307–6326, https://doi.org/https://doi.org/10.1029/2018JD029522, 570 2019.

Lubik, A., McKee, G., Chen, T., and Kosatsky, T.: Municipal Heat Response Planning in British Columbia, Canada, Tech. rep., ENVIRONMENTAL HEALTH SERVICES, BRITISH COLUMBIA CENTER FOR DISEASE CONTROL; NATIONAL COLLABORATING CENTRE FOR ENVIRONMENTAL HEALTH, British Columbia, Canada, 2017.

Menne, M. J., Durre, I., Vose, R. S., Gleason, B. E., and Houston, T. G.: An Overview of the Global Historical Climatology Network-Daily 575 Database, J. Atmos. Oceanic Technol., 29, 897–910, https://doi.org/10.1175/JTECH-D-11-00103.1, 2012.

Mueller, B. and Seneviratne, S. I.: Hot days induced by precipitation deficits at the global scale, Proceedings of the National Academy of Sciences, 109, 12 398–12 403, https://doi.org/10.1073/pnas.1204330109, 2012.

Neale, R. B., Gettelman, A., Park, S., Conley, A. J., Kinnison, D., Marsh, D., Smith, A. K., Vitt, F., Morrison, H., Cameron-smith, P., Collins, W. D., Iacono, M. J., Easter, R. C., Liu, X., Taylor, M. A., chieh Chen, C., Lauritzen, P. H., Williamson, D. L., Garcia, R., francois 580 Lamarque, J., Mills, M., Tilmes, S., Ghan, S. J., Rasch, P. J., and Meteorology, M.: Description of the NCAR Community Atmosphere Model (CAM 5.0), Tech. Note NCAR/TN-486+STR, Natl. Cent. for Atmos, in: 6of7 ZHAO ET AL.: AEROSOL FIE SIMULATED BY CAMS L08806, pp. 2009–038 451, 2010.

O'Neill, B. C., Tebaldi, C., van Vuuren, D. P., Eyring, V., Friedlingstein, P., Hurtt, G., Knutti, R., Kriegler, E., Lamarque, J.-F., Lowe, J., Meehl, G. A., Moss, R., Riahi, K., and Sanderson, B. M.: The Scenario Model Intercomparison Project (ScenarioMIP) for CMIP6, Geoscientific Model Development, 9, 3461–3482, https://doi.org/10.5194/gmd-9-3461-2016, 2016.

Pfleiderer, P., Schleussner, C.-F., Kornhuber, K., and Coumou, D.: Summer weather becomes more persistent in a 2 °C world, Nature Climate Change, 9, 666–671, https://doi.org/10.1038/s41558-019-0555-0, 2019.

Philip, S. Y., Kew, S. F., van Oldenborgh, G. J., Otto, F. E. L., Vautard, R., van der Wiel, K., King, A. D., Lott, F. C., Arrighi, J., Singh, R. P., and van Aalst, M. K.: A protocol for probabilistic extreme event attribution analyses, Advances in Statistical Climatology, Meteorology and Oceanography, 6, 177–203, https://doi.org/10.5194/ascmo-6-177-2020, 2020.

Routson, C. C., McKay, N. P., Kaufman, D. S., Erb, M. P., Goosse, H., Shuman, B. N., Rodysill, J. R., and Ault, T.: Mid-latitude net precipitation decreased with Arctic warming during the Holocene, Nature, 568, 83–87, https://doi.org/10.1038/s41586-019-1060-3, 2019.

Seneviratne, S. I., Corti, T., Davin, E. L., Hirschi, M., Jaeger, E. B., Lehner, I., Orlowsky, B., and Teuling, A. J.: Investigating soil moisture?climate interactions in a changing climate: A review, Earth-Science Reviews, 99, 125–161, https://doi.org/https://doi.org/10.1016/j.earscirev.2010.02.004, 2010.

Singh, R., Arrighi, J., Jjemba, E., Strachan, K., Spires, M., and Kadihasanoglu, A.: Heatwave Guide for Cities, Tech. rep., Red Cross Red Crescent Climate Centre., 2019.

Skamarock, C., Klemp, B., Dudhia, J., Gill, O., Liu, Z., Berner, J., Wang, W., Powers, G., Duda, G., Barker, D., and yu Huang, X.: A Description of the Advanced Research WRF Model Version 4, Tech. rep., NCAR, tech. Note NCAR/TN-556+STR, 145 pp, 2019.

Stewart, R. E., Betancourt, D., Davies, J. B., Harford, D., Klein, Y., Lannigan, R., Mortsch, L., O'Connell, E., Tang, K., and Whitfield, P. H.: A multi-perspective examination of heat waves affecting Metro Vancouver: now into the future, Natural Hazards, 87, 791–815, https://doi.org/10.1007/s11069-017-2793-7, 2017.

Stone, D. A., Christidis, N., Folland, C., Perkins-Kirkpatrick, S., Perlwitz, J., Shiogama, H., Wehner, M. F., Wolski, P., Cholia, S., Krishnan, H., Murray, D., Angélil, O., Beyerle, U., Ciavarella, A., Dittus, A., Quan, X.-W., and Tadross, M.: Experiment design of the International CLIVAR C20C+ Detection and Attribution project, Weather and Climate Extremes, 24, 100 206, https://doi.org/https://doi.org/10.1016/j.wace.2019.100206, 2019.

Stringfellow, M. and Wagle, D.: The Economics of Homelessness in Seattle and King County, McKinsey & Company, retrieved from: https://www.mckinsey.com/featured-insights/future-of-cities/the-economics-of-homelessness-in-seattle-and-king-county. (Accessed on: July 4, 2021), 2018.

Tang, Q., Zhang, X., and Francis, J. A.: Extreme summer weather in northern mid-latitudes linked to a vanishing cryosphere, Nature Climate Change, 4, 45–50, https://doi.org/10.1038/nclimate2065, 2014.

Taylor, K. E., Stouffer, R. J., and Meehl, G. A.: An Overview of CMIP5 and the Experiment Design, Bull. Amer. Met. Soc., 93, 485–498, https://doi.org/10.1175/BAMS-D-11-00094.1, 2011.

Thiery, W., Davin, E. L., Lawrence, D. M., Hirsch, A. L., Hauser, M., and Seneviratne, S. I.: Present-day irrigation mitigates heat extremes, Journal of Geophysical Research: Atmospheres, 122, 1403–1422, https://doi.org/10.1002/2016JD025740, 2017.

U.S. Census Bureau: American Housing Survey (AHS), retrieved from: https://www.census.gov/programs-surveys/ahs/data/interactive/ahstablecreator.html, 2019.

van Oldenborgh, G. J., van der Wiel, K., Kew, S., Philip, S., Otto, F., Vautard, R., King, A., Lott, F., Arrighi, J., Singh, R., and van Aalst, M.: Pathways and pitfalls in extreme event attribution, Climatic Change, 166, 13, https://doi.org/10.1007/s10584-021-03071-7, 2021.

620   Vautard, R., van Aalst, M. K., Boucher, O., Drouin, A., Haustein, K., Kreienkamp, F., van Oldenborgh, G. J., Otto, F. E. L., Ribes, A., Robin, Y., Schneider, M., Soubeyroux, J.-M., Stott, P. A., Seneviratne, S. I., Vogel, M. M., and Wehner, M. F.: Human contribution to the record-breaking June and July 2019 heat waves in Western Europe, Environ. Res. Lett., 15, 094 077, https://doi.org/10.1088/1748-9326/aba3d4, 2020.

Vavrus, S.: The Influence of Arctic Amplification on Mid-latitude Weather and Climate, Current Climate Change Reports, 4,
625   https://doi.org/10.1007/s40641-018-0105-2, 2018.

Vecchi, G. A., Delworth, T., Gudgel, R., Kapnick, S., Rosati, A., Wittenberg, A. T., Zeng, F., Anderson, W., Balaji, V., Dixon, K., et al.: On the seasonal forecasting of regional tropical cyclone activity, J. Climate, 27, 7994–8016, https://doi.org/10.1175/JCLI-D-14-00158.1, 2014.

Vincent, L. A., Hartwell, M. M., and Wang, X. L.: A Third Generation of Homogenized Temperature for Trend Analysis and Monitoring
630   Changes in Canada?s Climate, Atmosphere-Ocean, 58, 173–191, https://doi.org/10.1080/07055900.2020.1765728, 2020.

Wehrli, K., Guillod, B. P., Hauser, M., Leclair, M., and Seneviratne, S. I.: Identifying Key Driving Processes of Major Recent Heat Waves, Journal of Geophysical Research: Atmospheres, 124, 11 746–11 765, https://doi.org/https://doi.org/10.1029/2019JD030635, 2019.

Yang, W., Hsieh, T.-L., and Vecchi, G. A.: Hurricane annual cycle controlled by both seeds and genesis probability, Proceedings of the National Academy of Sciences, 118, https://doi.org/10.1073/pnas.2108397118, 2021.